Two inhibitory neuronal classes govern acquisition and recall of spinal sensorimotor adaptation

Authors: Simon Lavaud[1, 2], Charlotte Bichara[1, 2], Mattia D'Andola[1, 2], Shu-Hao Yeh[1, 2], Aya Takeoka[1, 2, 3, *]

Affiliations:

[1] VIB-Neuroelectronics Research Flanders (NERF), 3001 Leuven, Belgium

[2] KU Leuven, Department of Neuroscience and Leuven Brain Institute, 3000 Leuven, Belgium

[3]Imec, 3001, Leuven, Belgium

*Corresponding author. Email: aya.takeoka@nerf.be

Abstract:
Spinal circuits are central to movement adaptation, yet the mechanisms within the spinal cord responsible for acquiring and retaining behavior upon experience remain unclear. Using a simple conditioning paradigm, we find that dorsal inhibitory neurons are indispensable for adapting protective limb withdrawal behavior, by regulating the transmitting a specific set of somatosensory information to enhance the saliency of conditioning cues associated with limb position. In contrast, maintaining previously acquired motor adaptation required the ventral inhibitory Renshaw cells. Manipulating Renshaw cells does not impact the adaptation itself but flexibly alters the expression of adaptive behavior. These findings identify a circuit basis involving two distinct populations of spinal inhibitory neurons enabling lasting sensorimotor adaptation independently from the brain.

One-Sentence Summary:

Two distinct spinal inhibitory populations regulate adapting and maintaining protective limb withdrawal behavior in the absence of the brain.

Main text

The spinal cord executes and adjusts motor outputs by integrating information from multiple somatosensory channels, even without brain input (*1–3*). Moreover, the spinal cord exhibits autonomous lasting motor adjustments (sensorimotor learning) following repetitive practice in various motor tasks (*4–6*). Yet, how this is achieved is currently unknown.

The protective limb withdrawal conditioning paradigm is a powerful model for studying the principles of sensorimotor learning, where the nerve cord of insects and the spinal cord of rodents associate conditioning cues and limb position and, consequently, adjust motor output (*7*, *8*). Although this paradigm has revealed that the spinal cord exhibits motor adaptation and lasting conditioning effects (*9–11*), the underlying mechanisms remain elusive. Gaining insight into these mechanisms is essential to reveal the foundations of somatosensory integration for motor adaptation in health and recovery mechanisms after spinal cord injury.

The spinal cord comprises genetically diverse neuronal populations with distinct molecular markers, spatial positioning, and connectivity patterns with broad functional division into two categories: dorsal neurons, which regulate sensory transmission and processing, and ventral neurons, responsible for modulating motor output (*12–14*). Whereas the contributions of spinal neuronal types to coordinating rhythmic movements, such as locomotion and scratching, are relatively well characterized (*15–19*), their roles in lasting motor adaptation remain elusive. Among spinal neurons, inhibitory neurons serve diverse functions: dorsal inhibitory neurons regulate somatosensory input processing by providing presynaptic inhibition, thus controlling the saliency of information (*20*, *21*). Ventral inhibitory neurons, many of which directly synapse onto motor neurons, are essential for patterning and coordinating motor output activity (*17*, *22*, *23*).

However, whether and how functionally diverse inhibitory neurons might regulate adapting and expressing previously learned behavior remains unclear. In addition, the lack of approaches using in vivo spinal single-unit recordings in awake, behaving animals limits our grasp on how spinal neuronal activities represent learning.

The spinal cord adapts motor output and retains the behavior without the brain input

To assess learning in the spinal cord, we developed a kinematic framework of a motor adaptation paradigm inspired by studies on headless insects, where a certain leg position is associated with conditioning cues to avoid the stimuli (*8*). To characterize hindlimb movements, we used mice with completely transected spinal cord (~T10) and tracked hindlimb movements online (Fig.1A). We tested a pair of mice simultaneously by placing their upper bodies in separate harnesses while allowing their hindlimbs to move freely and virtually set the coordinates of their foot positions at rest as [x, y, z]=[0, 0, 0]. We established a closed-loop setup in which the detection of the foot below a 3mm threshold along the vertical z-axis from one pre-designated mouse triggered the simultaneous delivery of electrical stimuli to the hindlimb of both mice (Fig.1B). This setup created a paradigm in which one mouse in each pair received conditioning cues any time the foot was below 3mm while the other mouse received cues randomly regardless of its foot positions (Fig.1C, S1A, Movie S1). Consequently, one mouse associates conditioning cues and proprioceptive threshold information (subsequently referred to as learners), while the other does not (referred to as controls).

Both learners and controls responded to cues by elevating distal joints (fig.S2A). We computed 63 kinematic parameters (TableS1) and subsequent principal component analysis (PCA) revealed no sources of kinematic variability associated with the experimental groups (fig.S2B).

In contrast, learners and controls displayed divergent motor adaptations during the 10-minute trial. Learners adjusted and maintained their foot elevation above the threshold and reached the learning criterion (when no more cues are elicited) within 10 minutes, whereas controls did not show such adaptation (Fig.1D, S2C-D). Reconstructed Principal component 1 capturing the highest variance of the data set (TableS2) highlighted the difference between the two groups (Fig.1E) and revealed that foot positions were predictors of learning (fig.S2E-F). In addition to taking advantage of protective withdrawal behavior based on flexor contractions, imposing the threshold forcing limb extension also led to learning in a modified paradigm (fig.S3). These findings further demonstrate the spinal cord's capacity to associate conditioning cues and limb position to adapt motor output.

We next performed a reversal learning experiment on the original paradigm to determine whether the conditioning has a lasting impact on behavior following the single training. Here, the two groups underwent reversal learning where the contingency of limb position and conditioning cues were swapped during a switch session conducted 24 hours later (Fig.1F). We reasoned that if the previous experience did not have lasting effects, these mice would behave similarly to naive mice during the switch session. However, despite the new contingency rules, both groups adjusted their hindlimb positions during the switch session to match their training (Fig.1G-I, S2G). This result suggests that the spinal cord exhibits phenomena where a prior experience interferes with new learning, known as proactive interference.

Dorsal spinal neurons regulate learning

The spinal cord exhibiting learning and memory-based behavior prompted us to examine the neuronal substrates and circuit mechanisms mediating these abilities. To genetically target a distinct neuronal class among a wide variety of neurons during learning (excitatory vs. inhibitory and sensory (dorsal) vs. motor (ventral)-associated), we used six transgenic Cre driver lines marking transcriptionally defined progenitor domains (PD; Fig.2A). We crossed each line with $Tau^{LSL\text{-}FlpO\text{-}nlsLacZ}$ mice and injected an AAV-FRT-human diphtheria toxin receptor (hDTR) to bilateral L2-L5 segments to ablate PD-derived neurons using diphtheria toxin (DTX; Fig.2B, S4A-C). We then subjected PD-ablated (PD^{DTX}) mice to spinal transection and conditioning as learners (Fig.2C). All PD^{DTX} mice exhibited limb withdrawal in response to conditioning cues, indicating that ablating a single PD population did not impair motor function (fig.S4C-D). As such, the absence of motor adaptation is attributed to learning impairment.

We identified that ablating either *Tlx3*-expressing or *Ptf1α*-expressing populations perturbed learning. Conversely, ablating ventrally located cell types did not individually affect learning (Fig.2D-E). Acutely silencing spinal (caudal to the brainstem, Cdx^{Flp} dependent) PD cell types yielded the same conclusions using PD^{Cre}::Cdx^{Flp}::$Rosa^{LSL\text{-}FSF\text{-}hM4Di}$ mice with administration of C21, a selective agonist to engineered DREADD receptors (*24*) (fig.S4E). As *Tlx3*-expressing neurons transmit nociceptive stimuli (*25*), their ablation likely dampens instructive signals required for learning. Supporting this idea, $Tlx3^{DTX}$ and $Tlx3^{hM4Di}$ mice displayed hyposensitivity to cues, requiring a higher intensity of cues to induce limb withdrawal than wild-type mice (fig.S5A), likely dampening conditioning signals and contributing to compromised learning (Fig. 2F). In contrast, the specific mechanism by which *Ptf1α*-expressing neurons regulate learning remains unclear.

Neural activity of *Ptf1α*-expressing neurons diverges between learners and controls

We first performed electrophysiological recordings in awake, behaving mice using a Neuropixel probe coupled to an optic fiber (Fig.3A, S6A) and determined how *Ptf1α*-expressing activity differs between learner and control mice during the conditioning session using $Ptf1\alpha^{Cre}$::$Rosa^{LSL\text{-}ChR2(H134R)/EYFP}$ mice. This method enabled us to optically tag *Ptf1α*-expressing neurons and monitor neuronal activity along the dorsoventral axis during the conditioning (Fig.3B-C, S6B-F). Although we found a comparable number of isolated *Ptf1α*-expressing units along the DV axis in learners and controls (Fig.3D-E), their activity differed substantially. Around 60% of learner and control *Ptf1α*-expressing neurons exhibited activity modulation (Fig.3F, S7A), but the firing rate of upregulated learner *Ptf1α*-expressing neurons increased throughout the session, whereas firing did not increase in controls (Fig. 3G). However, the overall activity of the heterogeneous *Ptf1α*-expressing population (fig.S7B) is likely a poor predictor of learning; therefore, we subsequently focused on units that exhibited robust activity modulation (Z-score>10, ~15% of upregulated *Ptf1α*-expressing neurons in both learners and controls). The activity of these neurons was inversely correlated to the duration of pre-learning criterion only in learners (Fig.3G, S7C).

We next examined the activity *of Ptf1α*-negative units. Both learners and controls showed a notable (~45% of single units) increase in neuronal activity across the dorsoventral axis during conditioning, which suggests cues alone alter neuronal activities (fig.S8A-C). Among the upregulated *Ptf1α*-negative neurons, more neurons, especially those in the intermediate lamina, exhibited a

decreasing firing rate during the conditioning in learners compared to controls (fig.S8C-D). Thus, the findings suggest that the robust activity of *Ptf1α*-expressing neurons and the decreasing activity of *Ptf1α*-negative neurons underlie the learning process (Fig.3H).

Selective modulation of Aδ/C second-order neurons enhances the saliency of proprioceptive and Aδ/C association

Subsequently, we studied the link between *Ptf1α*-expressing neurons and presynaptic modulation of somatosensory afferents, a mechanism known to control the gain and discriminate acuity of information (*26*, *27*). We hypothesized that enhancing the saliency of vital information, the association of foot position and conditioning cues, by dampening noise via presynaptic inhibition was essential for facilitating this learning process. Therefore, we focused on second-order somatosensory neurons responding to cues monosynaptically. We reasoned that if *Ptf1α*-expressing neurons affect learning through presynaptic regulation of afferents, the modulation of second-order neurons might differ between learners and controls (Fig.4A).

Each identified second-order neuron responded to conditioning cues in distinct latencies, presumably representing different afferent inputs, such as proprioceptive afferents transmitting limb positions at the time of conditioning cues, Aβ, Aδ, and C afferents (*28–30*)(Fig.4B, S9A). We found no difference between learners and controls in the composition of second-order neurons categorized by their latencies or spatial distributions (fig.S9B-E). To determine whether second-order neurons are modulated differently between learners and controls, we characterized the consistency of their responses to cues and whether this probability changed during the session (Fig.4C). We identified no difference in the proportion of proprioceptive or Aβ second-order neurons that changed cue response probability between the two groups (Fig. 4D). In contrast, we found disparate modulation patterns in putative Aδ/C second-order neurons. Specifically, learner Aδ/C second-order units showed reduced response probability to cues immediately before the learning criterion (Fig.4D-E).

Why is the modulation of Aδ/C second-order neurons important? To facilitate the learning process, the local circuits must associate cues with proprioceptive limb position. Therefore, we next studied whether Aδ/C second-order neurons also receiving proprioceptive input (Fig.4F) are distinctly regulated from the rest of Aδ/C second-order neurons. We found only a few P+Aδ/C second-order units in controls; in contrast, a larger proportion of learners' P+Aδ/C second-order units increased response probability, and the effect was more pronounced compared to the remainder of Aδ/C second-order neurons (Fig.4G, S9E). Together, the Aδ/C submodality-specific responses in learners created a bias: information transmitted through P+Aδ/C second-order neurons gained prominence, while that of other Aδ/C second-order neurons was suppressed.

To determine whether the Aδ/C submodality-specific modulation is causally linked to *Ptf1α*-expressing neurons, we next employed chemogenetic silencing of *Ptf1α*-expressing neurons using *Ptf1α*^{Cre}::*Cdx*^{Flp}::*Rosa*$^{LSL\text{-}FSF\text{-}hM4Di}$ mice (Fig.4H). The silencing abolished the decrease in response probability of Aδ/C second-order neurons (Fig.4I), thus reducing learners' saliency of P+Aδ/C signal transmission. Together, these findings establish that *Ptf1α*^{ON} neurons are necessary for the decrease in response probability observed among Aδ/C second-order neurons, likely to enhance the saliency of P+Aδ/C information needed for motor adaptation (Fig.4J).

Ventral *En1*-expressing inhibitory population mediates interference by prior experience

Given that a single training session had a lasting impact during the reversal learning (Fig.1F-I), we employed cell type-specific silencing to identify the neuronal substrates responsible. We reasoned that if silencing a neuronal population during the reversal learning resembled that of naive mice, the population would be essential for interference (fig.S10A). Using *Ptf1α*^{Cre}::*Cdx*^{Flp}::*Rosa*$^{LSL\text{-}FSF\text{-}hM4Di}$ mice, we found that acute silencing of *Ptf1α*-expressing neurons during the reversal learning did not impact interference (fig.S10B). Likewise, we observed no interference by silencing *Tlx3*-expressing neurons. These results suggest that different cell types govern the conditioning and interference and that once the spinal cord learns to adapt motor output, the spinal cord readily does so, even with disrupted somatosensory transmission.

We next asked whether *DMRT3*-, *En1*-, *Shox2*-, *or Sim1*-expressing populations contribute to learning interference. Silencing a PD-expressing population at a time during the reversal learning led to $En1^{hM4Di}$ mice resembling naive mice, whereas silencing other cell types did not affect learning interference. This suggests that ventral inhibitory *En1*-expressing neurons interfere with new learning contingency after a single conditioning session (fig.S10B).

To determine whether proactive interference is attributable to *En1*-expressing neurons encoding previously learned behavior, we asked if manipulating *En1*-expressing neurons could affect the recall of limb withdrawal after a single conditioning trial. We used $En1^{Cre}$::$R26^{LSL\text{-}hM3Dq\text{-}DREADD}$ intercross ($En1^{hM3Dq}$ mice; Fig.5A) to acutely enhance the excitability of *En1*-expressing neurons during the recall session (Fig.5B). We found that the wildtype mice with or without C21 exhibited a ~20% reduction in conditioning cues to achieve the learning criterion during the recall session (Fig.5C-D). In contrast, $En1^{hM3Dq}$ +C21 mice exhibited a further ~80% reduction to reach the learning criterion. Conversely, we then used $En1^{hDM4i}$ mice and found lowering the excitability of *En1*-expressing neurons led to more cues to reach the learning criterion compared to conditioning day (Fig.5C-D).

Manipulating excitability of *En1*-expressing subpopulations flexibly alters recall of learned behavior

Since the *En1*-expressing population consists of heterogeneous neurons, we next investigated whether Renshaw cells (RCs) could encode this recall behavior. We reason that since RCs receive efference copy from motor neurons (MNs) and, in turn, modulate and gate MN activity (*31*, *32*), they are in a prime position to adjust limb position once learning is achieved. To test this hypothesis, we manipulated the excitability of Calbindin (CB)-positive RCs (*31*) by using CB^{Cre}::$En1^{Flp}$ mice crossed with Cre- and Flp-dependent DREADD activator (RC-FL^{hM3Dq}) or inhibitor ($Rosa^{LSL\text{-}FSF\text{-}hM4Di}$) lines (Fig.5E). Altering excitability of *En1*/CB-expressing RCs during the recall session was sufficient to either facilitate or disrupt reaching the learning criterion (Fig.5F, G). Neither the activation nor inhibition of overall *En1*-expressing or RCs during the conditioning session facilitated flexion behavior. This suggests that limb withdrawal during the recall trial cannot be attributed to motor response but rather to retrieving previously learned adaptation (fig.S4D, S11A-C). These findings suggest that RCs are crucial in modulating motor behavior during the recall phase once learning has occurred.

The findings led to at least two possible mechanisms by which RCs facilitated the recall behavior: directly through gating MNs or also through downstream Ia inhibitory neurons (IaIN) that control antagonistic MNs (*33*, *34*)(Fig.5H). Among the *En1*-expressing population, IaIN, a subset of RCs, and other unidentified $En1^{ON}$ neurons express Parvalbumin (PV; fig.S12A-D) (*31*). Therefore, we subjected $En1^{Cre}$::$Pvalb^{Flp}$::hM3Dq and $En1^{Cre}$::$Pvalb^{Flp}$::hM4Di mice to recall sessions. We reasoned that if RCs exclusively regulate recall via gating of MNs, activity manipulation of *En1*/PV-expressing neurons would partially recapitulate RC manipulation, as this approach targets only a fraction of RCs. Conversely, if RCs regulate recall by inhibiting IaIN that composes *En1*/PV-expressing neurons, enhancing the excitability of *En1*/PV-expressing neurons would likely counteract recall (Fig.5H).

Manipulation of *En1*/PV-expressing neurons contrasted with those observed with Renshaw cells. Enhancing the excitability of *En1*/PV-expressing neurons required more cues to achieve the learning criterion whereas inhibiting them necessitated fewer cues (Fig.5I). These results suggest that recall requires the contribution of RCs-IaIN-antagonistic MN circuits (Fig.5H). Collectively, our data indicate that two distinct inhibitory populations, *Ptf1α*- and *En1*-expressing cells, each regulate distinct learning phases (Fig.5J). Specifically, the initial process is steered by dorsally located *Ptf1α*-expressing neurons, which modulate Aδ/C afferent transmission to enhance the saliency of proprioceptive information. However, once the learning is achieved, the neuronal substrate responsible for recall shifts to ventrally located RC-IaIN circuits, crucial in coordinating antagonistic MN activities to execute learned limb flexion behavior.

Discussion

Although behavioral evidence of spinal learning and memory traces were established in the early 20th century, the identities of neurons and how they encode experience remain unclear (*5*, *35*). By taking advantage of a paradigm in which learning occurs within 10 minutes our study uncovers a cell type-specific mechanism. Circuits described here could provide the means for the spinal cord to contribute to lasting motor adaptation, which is likely essential for movement automaticity in health and recovery after spinal cord injury.

The spinal cord exhibits characteristics resembling various classical learning and memory definitions. For example, during reversal learning, learners experience proactive interference, defined as new learning hindered by existing memories (39). On the other hand, the behavior of control mice during the reversal learning may be interpreted as learned helplessness or latent inhibition, defined as a familiar stimulus requiring more time to elicit learning (*36*). The spinal circuits also exhibit extinction (*37*), a loss of conditioned response as an animal learns to uncouple a response from a stimulus (*38*). Such plasticity is likely crucial for maintaining flexibility, reducing the impact of outdated experiences, and replacing undesirable motor habits to improve motor skills.

Electrophysiological recording in awake, behaving animals unraveled submodality-specific modulation of Aδ/C afferents regulated by *Ptf1α*-expressing neurons and learning-related changes of *Ptf1α*-negative neurons, potentially including *En1*-expressing neurons. Of note, we found that none of the ventral PD populations examined singularly regulated motor adaptation despite the classical notion that ventral neurons are essential for motor-related functions. This observation is consistent with various sensorimotor learning models mediated by brain circuits, where sensory cues are critical (*39–41*). Together with previous pharmacological studies that alter the fidelity to somatosensory transmission (54, 55), our findings suggest that the spinal circuits also follow the fundamental principle of sensorimotor learning and highlight the critical role of sensory signals in motor adaptation. In contrast, a flexible combination of ventral neurons can execute the relatively rudimentary motor adaptation required in this paradigm.

From adaptation to recall of learned behavior, the neural substrate shifted from a dorsal to a ventral inhibitory PD class. We speculate that the spatial position of these neurons, particularly their exposure to somatosensory input, might be a critical factor for this functional division of learning and retention of learned behavior. Dorsal neurons encounter a continuous stream of somatosensory information that can vary from moment to moment, and they may be better equipped to meet environmental demands for adaptive behavior. On the other hand, ventral neurons may be more suited to execute appropriate output once familiar cues enter the spinal cord. Transcriptomic findings revealed that dorsal neurons express more plasticity-related genes, whereas ventral neurons exhibit enrichment in genes associated with structural stability (*42*). This further supports the link between the roles of spinal neurons in sensorimotor learning and their spatial positioning.

In summary, we identify two distinct neuronal populations as the substrates for limb withdrawal adaptation. The type of somatosensory information that regulates spinal motor adaptation is likely context-dependent. Nevertheless, our findings stress the importance of understanding the learning mechanisms mediated by spinal circuits, as they likely contribute to various motor learning processes and movement automaticity once motor skills are acquired. These concepts may also be relevant for rehabilitative training following spinal injuries and CNS disorders, where continuing adjustment of circuit-specific targeting during rehabilitative training facilitates distinct phases of motor recovery.

Acknowledgments

We thank Karin Jonckers, Antonio Folgado Laranjeira, Abigail Nugent, Nikky Corthout and VIB-KUL Center for Brain and Disease Research expert imaging facility, and many internship students for technical assistance, Fabian Kloosterman for advice on neural recordings and analysis, Martyn Goulding, Asli Ayaz, Vincent Bonin, Sha Liu, and members of Takeoka lab for discussions, Silvia Arber, Graziana Gatto, Karl Farrow and Joris de Wit for comments on the manuscript.

Funding

FWO-SB Ph.D. fellowship (S.B./1S56719N) to SL
MSCA Postdoctoral Fellowship (101067670) to CB
Taiwan-KU Leuven Ph.D. student fellowship (P1040) to SY
Wings for Life Spinal Cord Research Foundation (WFL-BE-15/22) to AT
FWO Research Grants (G096320N and G074823N) to AT

Competing interests: Authors declare that they have no competing interests.

Data and materials availability: All data are available in https://doi.org/10.5061/dryad.v9s4mw73n. All codes are available at https://github.com/takeokalabnerf/Spinal-conditioning_Lavaud-et-al.git.

References

1. H. Forssberg, S. Grillner, S. Rossignol, Phase dependent reflex reversal during walking in chronic spinal cats. *Brain Res.* **132**, 121–139 (1975).
2. A. Frigon, M.-F. Hurteau, Y. Thibaudier, H. Leblond, A. Telonio, G. D'Angelo, Split-Belt Walking Alters the Relationship between Locomotor Phases and Cycle Duration across Speeds in Intact and Chronic Spinalized Adult Cats. *J. Neurosci.* **33**, 8559–8566 (2013).
3. C. Heng, R. D. de Leon, The Rodent Lumbar Spinal Cord Learns to Correct Errors in Hindlimb Coordination Caused by Viscous Force Perturbations during Stepping. *J. Neurosci.* **27**, 8558–8562 (2007).
4. J. R. Wolpaw, C. L. Lee, Memory traces in primate spinal cord produced by operant conditioning of H-reflex. *J. Neurophysiol.* **61**, 563–572 (1989).
5. J. R. Wolpaw, Spinal cord plasticity in acquisition and maintenance of motor skills. *Acta Physiol.* **189**, 155–169 (2007).
6. H. Zhong, R. R. Roy, K. K. Nakada, S. Zdunowski, N. Khalili, R. D. de Leon, V. R. Edgerton, Accommodation of the Spinal Cat to a Tripping Perturbation. *Front. Physiol.* **3**, 112 (2012).
7. A. A. BUERGER, A. FENNESSY, Learning of Leg Position in Chronic Spinal Rats. *Nature* **225**, 751–752 (1970).
8. G. Horridge, Learning of leg position by headless insects. *Nature* (1962).
9. E. D. Crown, A. R. Ferguson, R. L. Joynes, J. W. Grau, Instrumental learning within the spinal cord: IV. Induction and retention of the behavioral deficit observed after noncontingent shock. *Behav. Neurosci.* **116**, 1032–1051 (2002).
10. R. L. Joynes, K. Janjua, J. W. Grau, Instrumental learning within the spinal cord: VI The NMDA receptor antagonist, AP5, disrupts the acquisition and maintenance of an acquired flexion response. *Behav. Brain Res.* **154**, 431–438 (2004).
11. K. M. Baumbauer, J. R. Huie, A. J. Hughes, J. W. Grau, Timing in the Absence of Supraspinal Input II: Regularly Spaced Stimulation Induces a Lasting Alteration in Spinal Function That Depends on the NMDA Receptor, BDNF Release, and Protein Synthesis. *J. Neurosci.* **29**, 14383–14393 (2009).
12. S. Arber, Motor Circuits in Action: Specification, Connectivity, and Function. *Neuron* **74**, 975–989 (2012).
13. O. Kiehn, Decoding the organization of spinal circuits that control locomotion. *Nat. Rev. Neurosci.* **17**, 224–238 (2016).
14. M. Goulding, Circuits controlling vertebrate locomotion: moving in a new direction. *Nat. Rev. Neurosci.* **10**, 507–518 (2009).
15. D. Satoh, C. Pudenz, S. Arber, Context-Dependent Gait Choice Elicited by EphA4 Mutation in Lbx1 Spinal Interneurons. *Neuron* **89**, 1046–1058 (2016).
16. S. Gosgnach, G. M. Lanuza, S. J. B. Butt, H. Saueressig, Y. Zhang, T. Velasquez, D. Riethmacher, E. M. Callaway, O. Kiehn, M. Goulding, V1 spinal neurons regulate the speed of vertebrate locomotor outputs. *Nature* **440**, 215–219 (2006).
17. J. Zhang, G. M. Lanuza, O. Britz, Z. Wang, V. C. Siembab, Y. Zhang, T. Velasquez, F. J. Alvarez, E. Frank, M. Goulding, V1 and V2b Interneurons Secure the Alternating Flexor-Extensor Motor Activity Mice Require for Limbed Locomotion. *Neuron* **82**, 138–150 (2014).
18. S. Perry, M. Larhammar, J. Vieillard, C. Nagaraja, M. M. Hilscher, A. Tafreshiha, F. Rofo, F. V. Caixeta, K. Kullander, Characterization of Dmrt3-Derived Neurons Suggest a Role within Locomotor Circuits. *J. Neurosci.* **39**, 1771–1782 (2019).
19. G. Gatto, S. Bourane, X. Ren, S. D. Costanzo, P. K. Fenton, P. Halder, R. P. Seal, M. D. Goulding, A Functional Topographic Map for Spinal Sensorimotor Reflexes. *Neuron* **109**, 91-104.e5 (2021).
20. J. N. Betley, C. V. E. Wright, Y. Kawaguchi, F. Erdélyi, G. Szabó, T. M. Jessell, J. A. Kaltschmidt, Stringent Specificity in the Construction of a GABAergic Presynaptic Inhibitory Circuit. *Cell* **139**, 161–174 (2009).
21. D. I. Hughes, M. Mackie, G. G. Nagy, J. S. Riddell, D. J. Maxwell, G. Szabó, F. Erdélyi, G. Veress, P. Szűcs, M. Antal, A. J. Todd, P boutons in lamina IX of the rodent spinal cord express

high levels of glutamic acid decarboxylase-65 and originate from cells in deep medial dorsal horn. *Proc. Natl. Acad. Sci.* **102**, 9038–9043 (2005).
22. L. S. Andersson, M. Larhammar, F. Memic, H. Wootz, D. Schwochow, C.-J. Rubin, K. Patra, T. Arnason, L. Wellbring, G. Hjälm, F. Imsland, J. L. Petersen, M. E. McCue, J. R. Mickelson, G. Cothran, N. Ahituv, L. Roepstorff, S. Mikko, A. Vallstedt, G. Lindgren, L. Andersson, K. Kullander, Mutations in DMRT3 affect locomotion in horses and spinal circuit function in mice. *Nature* **488**, 642–646 (2012).
23. A. E. Talpalar, J. Bouvier, L. Borgius, G. Fortin, A. Pierani, O. Kiehn, Dual-mode operation of neuronal networks involved in left–right alternation. *Nature* **500**, 85–88 (2013).
24. J. Bonaventura, M. A. G. Eldridge, F. Hu, J. L. Gomez, M. Sanchez-Soto, A. M. Abramyan, S. Lam, M. A. Boehm, C. Ruiz, M. R. Farrell, A. Moreno, I. M. G. Faress, N. Andersen, J. Y. Lin, R. Moaddel, P. J. Morris, L. Shi, D. R. Sibley, S. V. Mahler, S. Nabavi, M. G. Pomper, A. Bonci, A. G. Horti, B. J. Richmond, M. Michaelides, High-potency ligands for DREADD imaging and activation in rodents and monkeys. *Nat. Commun.* **10**, 4627 (2019).
25. Y. Xu, C. Lopes, Y. Qian, Y. Liu, L. Cheng, M. Goulding, E. E. Turner, D. Lima, Q. Ma, Tlx1 and Tlx3 Coordinate Specification of Dorsal Horn Pain-Modulatory Peptidergic Neurons. *J. Neurosci.* **28**, 4037–4046 (2008).
26. J. C. Eccles, R. F. Schmidt, W. D. Willis, Presynaptic inhibition of the spinal monosynaptic reflex pathway. *J. Physiol.* **161**, 282–297 (1962).
27. P. Rudomin, R. F. Schmidt, Presynaptic inhibition in the vertebrate spinal cord revisited. *Exp. Brain Res.* **129**, 1–37 (1999).
28. P. R. Burgess, E. R. Perl, Myelinated afferent fibres responding specifically to noxious stimulation of the skin. *J. Physiol.* **190**, 541–562 (1967).
29. D. M. Cain, S. G. Khasabov, D. A. Simone, Response Properties of Mechanoreceptors and Nociceptors in Mouse Glabrous Skin: An In Vivo Study. *J. Neurophysiol.* **85**, 1561–1574 (2001).
30. J. Walcher, J. Ojeda-Alonso, J. Haseleu, M. K. Oosthuizen, A. H. Rowe, N. C. Bennett, G. R. Lewin, Specialized mechanoreceptor systems in rodent glabrous skin. *J Physiol* **596**, 337923 (2018).
31. F. J. Alvarez, P. C. Jonas, T. Sapir, R. Hartley, M. C. Berrocal, E. J. Geiman, A. J. Todd, M. Goulding, Postnatal phenotype and localization of spinal cord V1 derived interneurons. *J. Comp. Neurol.* **493**, 177–192 (2005).
32. J. C. Eccles, P. Fatt, K. Koketsu, Cholinergic and inhibitory synapses in a pathway from motor-axon collaterals to motoneurones. *J. Physiol.* **126**, 524–562 (1954).
33. H. Hultborn, S. Lindström, H. Wigström, On the function of recurrent inhibition in the spinal cord. *Exp. Brain Res.* **37**, 399–403 (1979).
34. H. Hultborn, E. Jankowska, S. Lindström, Recurrent inhibition from motor axon collaterals of transmission in the Ia inhibitory pathway to motoneurones. *J. Physiol.* **215**, 591–612 (1971).
35. J. R. Wolpaw, A. M. Tennissen, Activity-dependent spinal cord plasticity in health and disease. *Annu. Rev. Neurosci.* **24**, 807–843 (2001).
36. R. E. Lubow, A. U. Moore, Latent inhibition: The effect of nonreinforced pre-exposure to the conditional stimulus. *J. Comp. Physiol. Psychol.* **52**, 415–419 (1959).
37. S. Lavaud, M. D'Andola, C. Bichara, A. Takeoka, Electrophysiological signatures reveal spinal intrinsic learning mechanisms for a lasting sensorimotor adaptation. *BioRxiv*, doi: 10.1101/2022.03.30.486422 (2022).
38. N. Guttman, Operant conditioning, extinction, and periodic reinforcement in relation to concentration of sucrose used as reinforcing agent. *J. Exp. Psychol.* **46**, 213–224 (1953).
39. J. W. Krakauer, P. Mazzoni, Human sensorimotor learning: adaptation, skill, and beyond. *Curr. Opin. Neurobiol.* **21**, 636–644 (2011).
40. D. M. Wolpert, J. Diedrichsen, J. R. Flanagan, Principles of sensorimotor learning. *Nat. Rev. Neurosci.* **12**, 739–751 (2011).
41. M. Kawato, Internal models for motor control and trajectory planning. *Curr. Opin. Neurobiol.* **9**, 718–727 (1999).

42. D. E. Russ, R. B. P. Cross, L. Li, S. C. Koch, K. J. E. Matson, A. Yadav, M. R. Alkaslasi, D. I. Lee, C. E. L. Pichon, V. Menon, A. J. Levine, A harmonized atlas of mouse spinal cord cell types and their spatial organization. *Nat. Commun.* **12**, 5722 (2021).
43. S. M. Glasgow, R. M. Henke, R. J. MacDonald, C. V. E. Wright, J. E. Johnson, Ptf1a determines GABAergic over glutamatergic neuronal cell fate in the spinal cord dorsal horn. *Development* **132**, 5461–5469 (2005).
44. S. Perry, M. Larhammar, J. Vieillard, C. Nagaraja, M. M. Hilscher, A. Tafreshiha, F. Rofo, F. V. Caixeta, K. Kullander, Characterization of Dmrt3-Derived Neurons Suggest a Role within Locomotor Circuits. *J. Neurosci.* **39**, 1771–1782 (2019).
45. T. Sapir, E.J. Geiman, Z. Wang, T. Velasquez, S. Mitsui, Y Yoshihara, E. Frank, F.J. Alvarez, and M. Goulding. (2004). Pax6 and engrailed 1 regulate two distinct aspects of renshaw cell development. J. Neurosci. 24, 1255–1264
46. J. B. Bikoff, M. I. Gabitto, A. F. Rivard, E. Drobac, T. A. Machado, A. Miri, S. Brenner-Morton, E. Famojure, C. Diaz, F. J. Alvarez, G. Z. Mentis, T. M. Jessell, Spinal Inhibitory Interneuron Diversity Delineates Variant Motor Microcircuits. *Cell* **165**, 207–219 (2016).
47. K. J. Dougherty, L. Zagoraiou, D. Satoh, I. Rozani, S. Doobar, S. Arber, T. M. Jessell, O. Kiehn, Locomotor Rhythm Generation Linked to the Output of Spinal Shox2 Excitatory Interneurons. *Neuron* **80**, 920–933 (2013).
48. Y. Zhang, S. Narayan, E. Geiman, G. M. Lanuza, T. Velasquez, B. Shanks, T. Akay, J. Dyck, K. Pearson, S. Gosgnach, C.-M. Fan, M. Goulding, V3 Spinal Neurons Establish a Robust and Balanced Locomotor Rhythm during Walking. *Neuron* **60**, 84–96 (2008).
49. S. Bourane, K. S. Grossmann, O. Britz, A. Dalet, M. G. Del Barrio, F. J. Stam, L. Garcia-Campmany, S. Koch, M. Goulding, Identification of a Spinal Circuit for Light Touch and Fine Motor Control. *Cell* **160**, 503–515 (2015).
50. C. Pivetta, M. S. Esposito, M. Sigrist, S. Arber, Motor-Circuit Communication Matrix from Spinal Cord to Brainstem Neurons Revealed by Developmental Origin. *Cell* **156**, 537–548 (2014).
51. M. Tripodi, A. E. Stepien, S. Arber, Motor antagonism exposed by spatial segregation and timing of neurogenesis. *Nature* **479**, 61–66 (2011).
52. S. Bourane, B. Duan, S. C. Koch, A. Dalet, O. Britz, L. Garcia-Campmany, E. Kim, L. Cheng, A. Ghosh, Q. Ma, M. Goulding, Gate control of mechanical itch by a subpopulation of spinal cord interneurons. *Science* **350**, 550–554 (2015).
53. A. Takeoka, S. Arber, Functional Local Proprioceptive Feedback Circuits Initiate and Maintain Locomotor Recovery after Spinal Cord Injury. *Cell Rep.* **27**, 71-85.e3 (2019).
54. L. Ruder, A. Takeoka, S. Arber, Long-Distance Descending Spinal Neurons Ensure Quadrupedal Locomotor Stability. *Neuron* **92**, 1063–1078 (2016).
55. A. Escalante, R. Klein, Spinal Inhibitory Ptf1a-Derived Neurons Prevent Self-Generated Itch. *Cell Rep.* **33**, 108422 (2020).
56. M. J. Farrar, I. M. Bernstein, D. H. Schlafer, T. A. Cleland, J. R. Fetcho, C. B. Schaffer, Chronic in vivo imaging in the mouse spinal cord using an implanted chamber. *Nat. Methods* **9**, 297–302 (2012).
57. C. Stringer, M. Pachitariu, N. Steinmetz, C. B. Reddy, M. Carandini, K. D. Harris, Spontaneous behaviors drive multidimensional, brainwide activity. *Science* **364**, 255 (2019).
58. C. Rossant, S. N. Kadir, D. F. M. Goodman, J. Schulman, M. L. D. Hunter, A. B. Saleem, A. Grosmark, M. Belluscio, G. H. Denfield, A. S. Ecker, A. S. Tolias, S. Solomon, G. Buzsáki, M. Carandini, K. D. Harris, Spike sorting for large, dense electrode arrays. *Nat. Neurosci.* **19**, 634–641 (2016).
59. A. C. Snyder, M. J. Morais, M. A. Smith, Dynamics of excitatory and inhibitory networks are differentially altered by selective attention. *J. Neurophysiol.* **116**, 1807–1820 (2016).
60. E. K. Lee, H. Balasubramanian, A. Tsolias, S. U. Anakwe, M. Medalla, K. V. Shenoy, C. Chandrasekaran, Non-linear dimensionality reduction on extracellular waveforms reveals cell type diversity in premotor cortex. *eLife* **10**, e67490 (2021).

61. S. H. Sun, A. Almasi, M. Yunzab, S. Zehra, D. G. Hicks, T. Kameneva, M. R. Ibbotson, H. Meffin, Analysis of extracellular spike waveforms and associated receptive fields of neurons in cat primary visual cortex. *J. Physiol.* **599**, 2211–2238 (2021).
62. L. Cui, X. Miao, L. Liang, I. Abdus-Saboor, W. Olson, M. S. Fleming, M. Ma, Y.-X. Tao, W. Luo, Identification of Early RET+ Deep Dorsal Spinal Cord Interneurons in Gating Pain. *Neuron* **91**, 1137–1153 (2016).
63. M. W. Berry, M. Browne, A. N. Langville, V. P. Pauca, R. J. Plemmons, Algorithms and applications for approximate nonnegative matrix factorization. *Comput. Stat. Data Anal.* **52**, 155–173 (2007).
64. M. W. Doyle, M. C. Andresen, Reliability of Monosynaptic Sensory Transmission in Brain Stem Neurons In Vitro. *J Neurophysiol* **85**, 2213–2223 (2001).
65. J. Hachisuka, K. M. Baumbauer, Y. Omori, L. M. Snyder, H. R. Koerber, S. E. Ross, Semi-intact ex vivo approach to investigate spinal somatosensory circuits. *Elife* **5**, e22866 (2016).
66. J. Walcher, J. Ojeda-Alonso, J. Haseleu, M. K. Oosthuizen, A. H. Rowe, N. C. Bennett, G. R. Lewin, Specialized mechanoreceptor systems in rodent glabrous skin. *J Physiol* **596**, 337923 (2018).
67. Y. Roudaut, A. Lonigro, B. Coste, J. Hao, P. Delmas, M. Crest, Touch sense. *Channels* **6**, 234–245 (2012).
68. B. Efron, R. Tibshirani, Statistical Data Analysis in the Computer Age. *Science* **253**, 390–395 (1991).
69. V. Saravanan, G. J. Berman, S. J. Sober, Application of the hierarchical bootstrap to multi-level data in neuroscience. *Neurons, Behav., data Anal. theory* **3** (2020).
70. N. Cliff, Dominance Statistics: Ordinal Analyses to Answer Ordinal Questions. *Psychol. Bull.* **114**, 494–509 (1993).

Figure legends

Figure 1. The spinal cord adapts and displays a lasting impact on motor output.
(A, B) Experimental timeline (A) and scheme of the closed-loop setup for the online reconstruction of hindlimb joints and delivery of conditioning cues along defined orthogonal 3D axis (B). Five high-speed cameras reconstruct joint positions online in 3D space to trigger conditioning cues (30Hz, ~0.2 mA), when a learner's foot is below the predetermined Z-axis threshold. cSTX: complete spinal transection. M-L: medio-lateral, A-P: anterior-posterior, V: vertical.
(C) Representative reconstructions of foot positions for a pair of learner and control mice during a conditioning session. Gray vertical solid lines indicate conditioning cue delivery, and red dotted lines the +3 mm conditioning cue threshold. The insets show the first 10 sec of the trial. Learning criterion refers to the time point in which no more conditioning cues are elicited because limb flexion is maintained above the threshold. The data is down-sampled to 1Hz for visualization. Yellow dots show foot positions when conditioning cues are elicited.
(D) Mean foot position of learner (magenta) and control (cyan) mice during the first and last 10 seconds of the ten-minute conditioning trial along the Z-axis (n=25 each). A red dotted line indicates the conditioning cue threshold; 0 shows the resting position at the beginning of a trial. The shaded area represents 1 SD.
(E) PC analysis describes features of the limb kinematics in the new PC1-2 space for learning (each dot represents one mouse, n=25 each). Least-square elliptical fitting (95% confidence) is shown. Histogram plot reporting mean values of measured PC1 scores (Student's paired t-test, ***$p<0.001$).
(F) Timeline of reversal learning in which training is followed by a switch experiment where contingency of foot position and conditioning cues are reversed.
(G) Mean foot positions of group 1 (different shades of magenta) and group 2 (different shades of cyan) mice over ten-minute conditioning (Training) and switch (reversal learning, 24h after conditioning) sessions (n=7 each). The data are down-sampled to 1Hz. The shaded area represents 1 SD.
(H) PC analysis describes features of the limb kinematics in the new PC1-2 space for learning (each dot represents one mouse, n=7 each). Histogram plot reporting mean values of measured PC1 scores (Student's paired t-test, $p>0.05$).
Error bars represent SEM. a.u: arbitrary unit.

Figure 2. Restricted progenitor domain origin of dorsal neurons regulates spinal learning.
(A) Scheme of spinal cord progenitor domains (dI1-dI6, V0-V3, and MN) and transcription factor code of analyzed excitatory neurons (dI3, dI5: *Tlx3*, V2: *Shox2*, and V3: *Sim1*) and inhibitory neurons (dI4: *Ptf1*α, dI6: *DMRT3,* V1: *En1*).
(B, C) Timeline and targeting strategy for PD^{DTX}-specific kinematic analyses. PD: Progenitor domain, DTR: Diphtheria toxin receptor, DTX: Diphtheria toxin, cSTX: complete spinal cord transection.
(D) Average foot positions of PD^{DTX} mice along the Z-axis over the first eight minutes (n=5 each except n=4 for $Tlx3^{DTX}$). 0 indicates a normalized resting position at the beginning of the trial. The data is plotted at 1Hz. The shaded area represents 1 SD. The color coding is the same as 3A.
(E) PC analysis applied to learning parameters captures the learning phenomena for all but $Tlx3^{DTX}$ and $Ptf1\alpha^{DTX}$ mice. Histogram plot reporting mean values of measured PC1 scores. (Comparison to wild-type learner mice: $Tlx3^{DTX}$ and $Ptf1\alpha^{DTX}$: Student's unpaired two-sample *t*-test, ***$p<0.001$, $DMRT3^{DTX}$, $En1^{DTX}$, $Shox2^{DTX}$ and $Sim1^{DTX}$: $p>0.05$). Each dot represents one mouse. Color coding is the same as 3D. Gray dots indicate learners and white dots indicate controls.
(F) A circuit model based on ablation where the ablating excitatory *Tlx3*-expressing neurons dampen the transmission of conditioning cues, whereas ablating inhibitory *Ptf1*α-expressing neurons disrupt the gating of somatosensory information required for learning.
Error bars represent SEM.

Figure 3. Activity dynamics of *Ptf1*α-expressing neurons differ between learner and control groups.

(A) Left: Scheme of the vertebral column-fixed preparation for electrophysiology recording setup in awake, behaving mice with a custom-designed Neuropixel (NPXL) holder. Right: Representative reconstruction of *Ptf1α*-expressing neurons along the dorsoventral axis in the mouse spinal cord (40μm section; half of the spinal cord is shown), the position of the Neuropixel probe, and an optic fiber. Each purple dot represents one *Ptf1α*-expressing neuron.
(B) Experimental timeline of the *in vivo* awake behaving electrophysiology experiment.
(C) Foot position (top) and example raw spiking data (bottom) during the first 1.5 seconds of a conditioning trial from a learner mouse. Red vertical lines indicate conditioning cue delivery, and the red dotted line is the +3 mm threshold. Conditioning cue delivery intervals shown here are 349, 369, 353, and 381 ms.
(D) Example of an opto-tagged *Ptf1α*-expressing neuron. Top: Raster plot of an isolated unit responding to a 10 ms light stimulation aligned to the stimulation onsets (0.1 ms time bins). Bottom: Peristimulus Time Histograms of the same unit. Bottom right: The overlay of randomly chosen 300 spike waveforms of the *Ptf1α*-expressing neuron.
(E) Spatial locations of opto-tagged *Ptf1α*-expressing neurons in learners and controls are consistent with expected anatomical locations (learners: n = 65, controls: n = 65 units).
(F) Two example units (one each from a pair of learner and control) and their activities aligned to conditioning cues (red vertical lines). Windows of pre (the period with conditioning cues) and post (no cues) learning criterion is shown with black dotted lines.
(G) Left: Z-score transformed firing rates of upregulated *Ptf1*α-expressing neurons in learners and controls (n= 37, 34 units respectively), normalized to the baseline. Shaded areas indicated in SEM. Inset: The slope of activity modulation (Mann-Whitney test, $*p<0.05$). Right: Of the upregulated *Ptf1*α-expressing neurons, highly modulated units (z score>10 compared to the baseline) from learners (n= 9) are broadly aligned to learning (time in which 90% of conditioning cues are delivered), while that of controls (n= 9) are not.
(H) Summary diagram of conditioning cue contingencies, *Ptf1*α-expressing and others' neuronal activities, and behavioral outcome.

Figure 4. Conditioning cues modulate Aδ/C second-order neurons differently in learners and controls.
(A) The connectivity scheme of *Ptf1*α-expressing neurons where they modulate second-order neurons via gating of somatosensory afferents.
(B) Top left: Range of expected response latencies to conditioning cues by second-order neurons receiving monosynaptic input from various somatosensory afferents. Top middle: Distribution of units with observed response latencies of second-order neurons. Learners and controls are combined. Raster plots and peristimulus time histograms of four representative neurons, receiving monosynaptic input from presumed proprioceptive (top right) Aβ (bottom left), Aδ (bottom middle), and C (bottom right) afferents.
(C) Scheme and representative units that show an increase, decrease, or no change of response probability to conditioning cues.
(D) The proportion of Proprioceptive, Aβ, and Aδ/C second-order units that exhibit increase, decrease, or no change of response probability to conditioning cues (Pearson's chi-squared test, $*p<0.05$). The decrease (%) of response probability from the first to the last 10% conditioning cues of Aδ/C second-order units (Mann-Whitney test, $*p<0.05$).
(E) The first and last 20% of conditioning cues in 10% bin, and response probability of Aδ/C second-order units (ANOVA or Kruskal Walis test for repeated measurement and Dunn-Sidak posthoc test, $p< 0.05$; $***p< 0.001$). Median ± quartiles are shown.
(F) Raster plots and peristimulus time histograms of a representative neuron receiving monosynaptic input from presumed proprioceptive and Aδ/C afferents. Pie charts indicate the proportion of Aδ/C second-order units also receiving proprioceptive afferent input.
(G) The proportion of Aδ/C and P+Aδ/C second-order units that exhibit increase, decrease, or no change of response probability to conditioning stimuli (Pearson's chi-squared test, $*p<0.05$). The

change (%) of response probability from the first to the last 10% conditioning cues of Aδ/C and P+Aδ/C second-order units (Student's unpaired two-sample *t*-test, $*p<0.05$).
(H) Scheme of acute silencing of *Ptf1*α-expressing neurons and the effect on Aδ/C second order neuron modulation.
(I) The proportion of Aδ/C second-order units exhibiting a diverse change in response probability with acute *Ptf1*α-expressing silencing during the conditioning trial. Asterisks indicate statistical differences between the learner group with or without *Ptf1*α-expressing neuron silencing (Pearson's chi-squared test, $**p<0.01$).
(J) Circuit model of *Ptf1*α-expressing neurons regulating the Aδ/C second-order transmission to enhance the saliency of proprioceptive and Aδ/C transmission and integration.

Figure 5. Activity manipulation of the inhibitory *En1*-expressing subpopulations flexibly facilitates or disrupts recalling learned behavior.
(A) Representative image of *En1*-expressing neurons expressing hM3Dq-DREADD activator ($En1^{hM3Dq}$) in the lumbar spinal cord. Half of the spinal cord is shown.
(B) Experimental timeline of conditioning and recall sessions, experimental group, and C21 administration schedule.
(C) Example foot traces of the first 10 seconds of wild-type (top left), $En1^{hMD3q}$ (top right), and $En1^{hMD4i}$ (bottom left) mice during the conditioning and the recall session.
(D) The number of conditioning cues required to achieve the learning criterion. Asterisks denote the statistical difference between days 1 and 2, and # denotes the statistical difference compared to the control day 2 (Wilcoxson matched-paired signed rank test or Mann-Whitney test, $*,^{\#}p< 0.05$, $**,^{\#\#}p< 0.01$, $***p< 0.001$). * denotes difference between days 1 and 2, # denotes differences between day2 wildtype and *En1*-expressing neuron manipulation.
(E) Genetically tractable *En1*-expressing subpopulation, Calbindin (CB)-expressing Renshaw Cells (RC; dark green), genetic targeting approach and a representative image of *En1*/CB-expressing neurons expressing hM3Dq-DREADD activator ($En1/CB^{hM3Dq}$; yellow) in the lumbar spinal cord. *En1*-expressing non-RC are shown in yellow.
(F) Example foot traces of the first 10 seconds of $En1/CB^{hM3Dq}$ mice during the conditioning and the recall session.
(G) The number of conditioning cues required to achieve the learning criterion (Wilcoxson matched-paired signed rank test, $**p<0.01$, $*p<0.05$).
(H) Previously described circuit connectivity of Renshaw cells to MNs, and Renshaw cells, Ia inhibitory neurons to antagonistic MNs.
(I) The number of conditioning cues required to achieve the learning criterion (Wilcoxson matched paired signed-rank test, $*p<0.05$).
(J) Proposed circuit model from motor adaptation to recall of learned behavior.

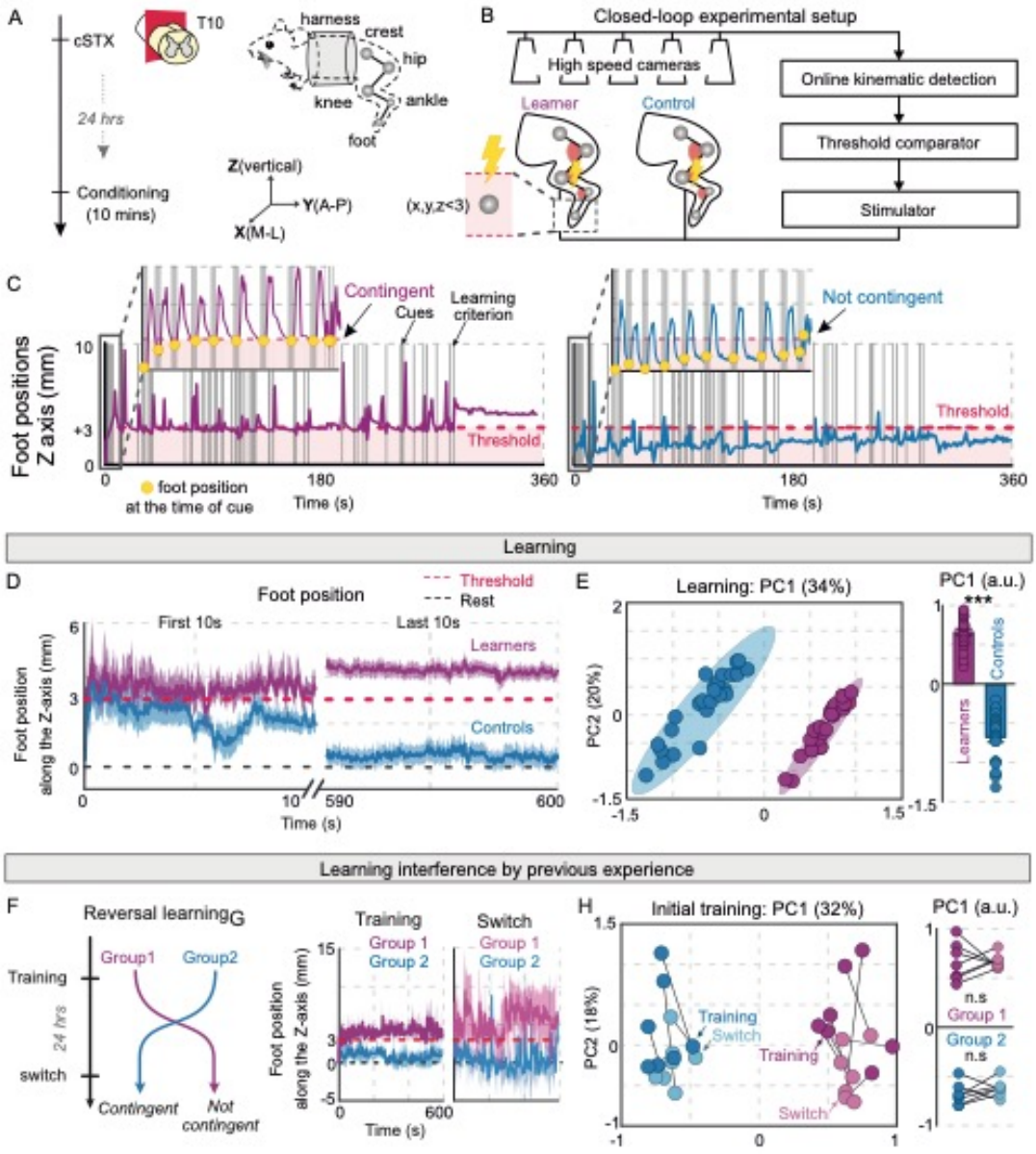

Figure 1. The spinal cord adapts and displays a lasting impact on motor output.

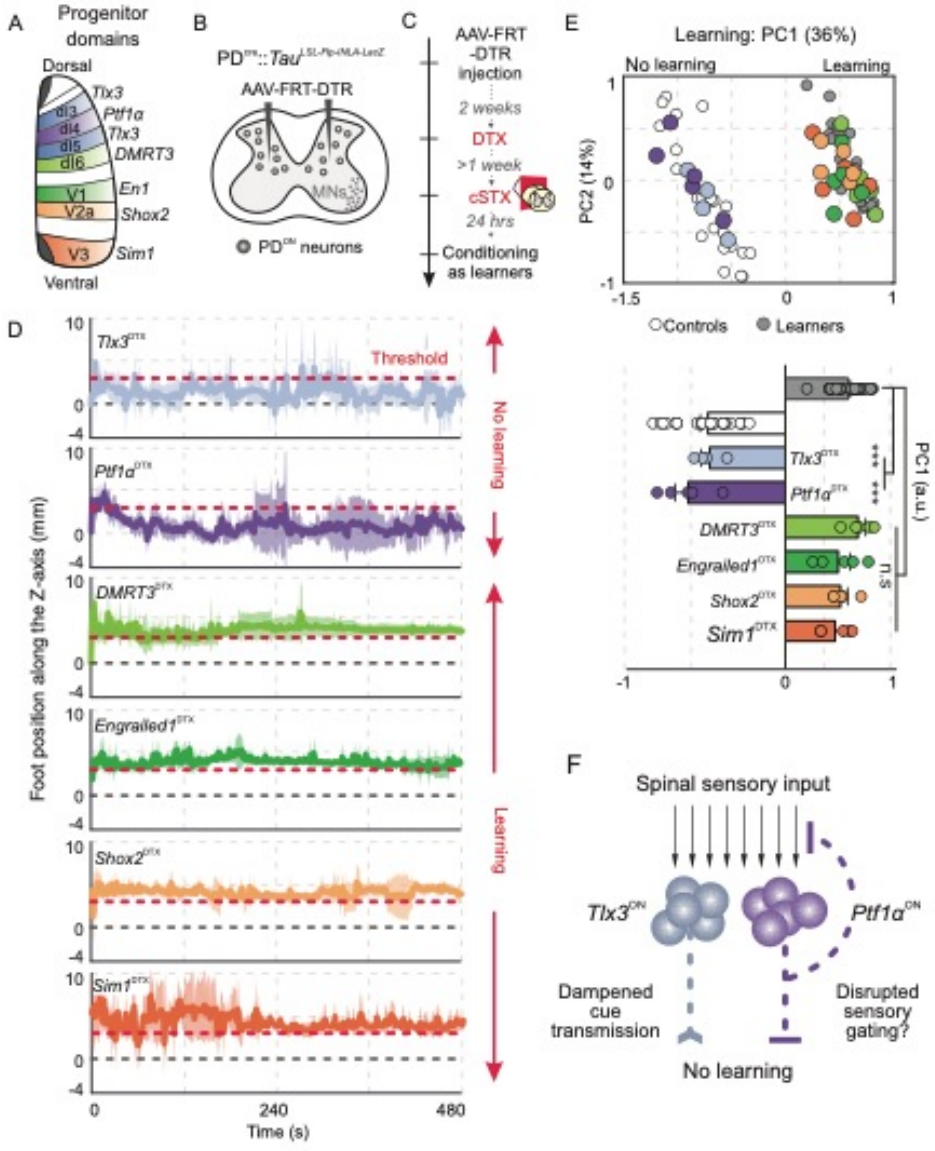

Figure 2. Restricted progenitor domain origin of dorsal neurons regulates spinal learning.

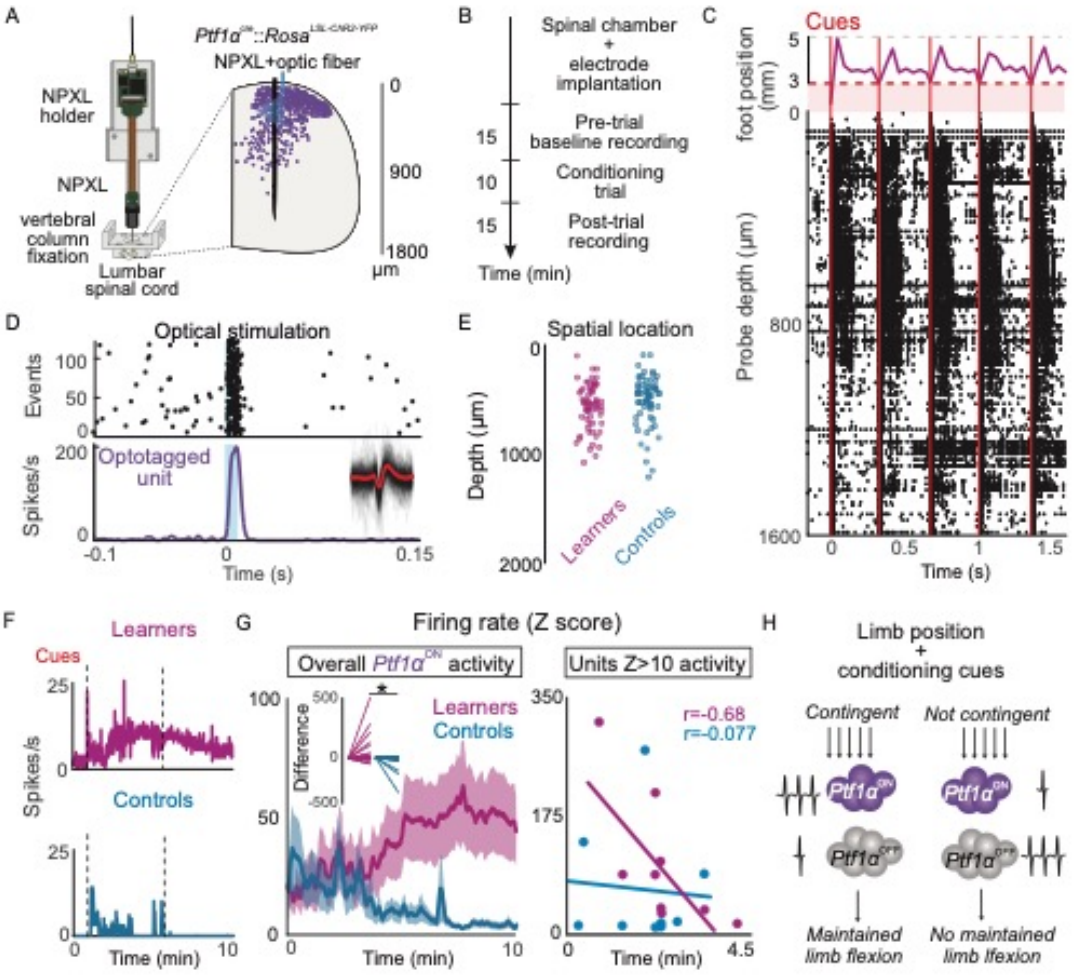

Figure 3. *Ptf1α*^{ON} activity dynamics differ between learner and control groups.

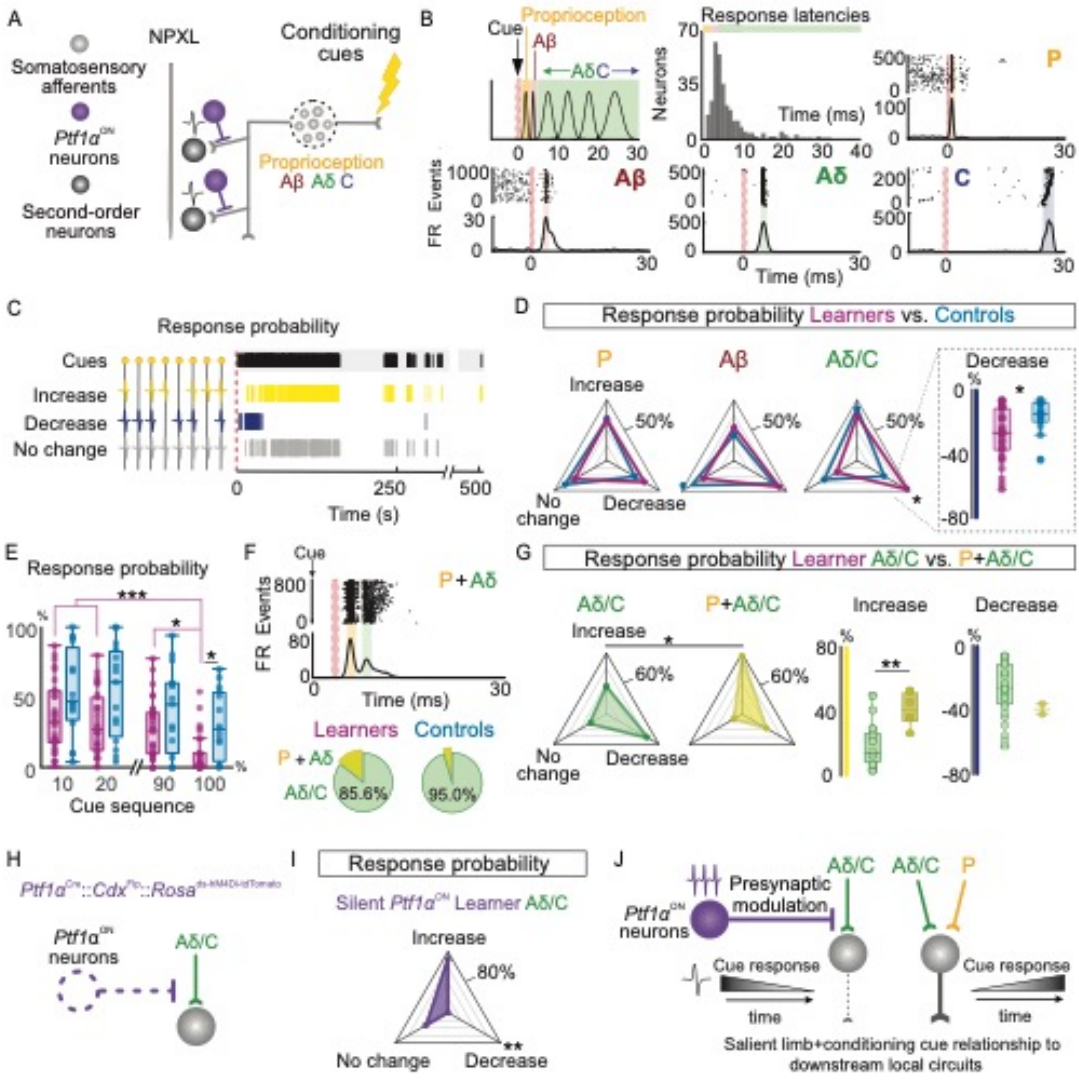

Figure 4. Conditioning cues modulate Aδ/C second-order neurons differently in learners and controls.

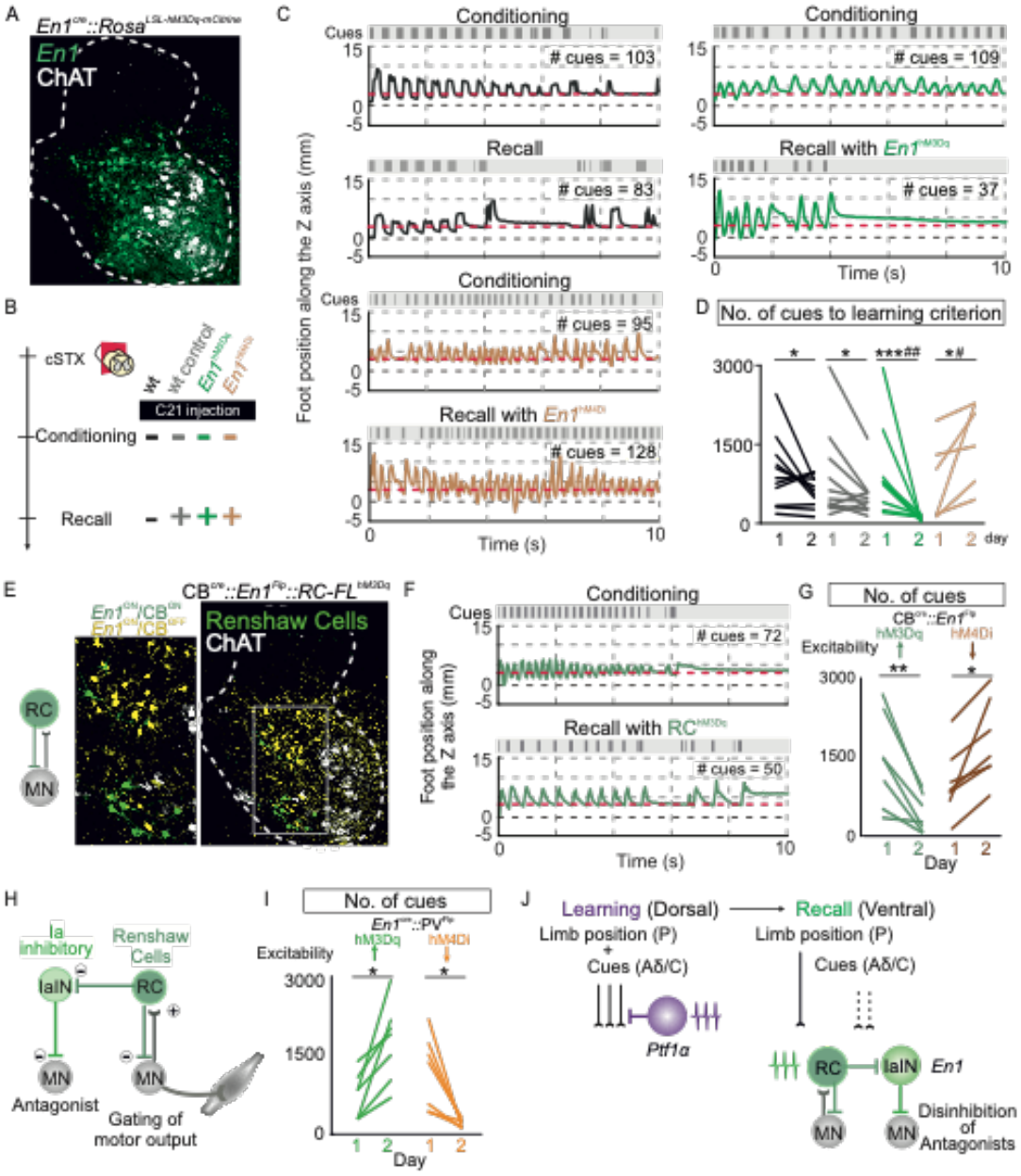

Figure 5. Activity manipulation of the inhibitory *En1*^{ON} subpopulations flexibly facilitates or disrupts recalling learned behavior.

Science
AAAS

Supplementary Materials for

Two inhibitory neuronal classes govern acquisition and recall of spinal sensorimotor adaptation.

Authors: Simon Lavaud, Charlotte Bichara, Mattia D'Andola, Shu-Hao Yeh, Aya Takeoka

*Corresponding author. Email: aya.takeoka@nerf.be

The PDF file includes:

Materials and Methods
Figs. S1 to S12
Tables S1 to S2

Other Supplementary Materials for this manuscript include the following:

Movies S1

Materials and Methods

Mice

Wild-type C57Bl6 (JAX 000664), *Tlx3*^{Cre} (Genesat, 041158-UCD), *Ptf1a*^{Cre} (*43*), *DMRT3*^{Cre} (*44*), *Engrailed1*^{Cre} (*45*), *Engrailed1*^{Flp} (*46*), *Shox2*^{Cre} (*47*), *Sim1*^{Cre} (*48*), Calbindin^{Cre} (JAX 028532), Pvalb^{Flp} (JAX 022730), *hCdx2*^{FlpO} (*49*), *Tau*$^{LSL\text{-}FlpO\text{-}INLA}$ (*50*), *Tau*$^{LSL\ or\ Floxed\text{-}DTR\text{-}IRES\text{-}nlsLacZ}$ (*51*), *R26*$^{LSL\text{-}hM3Dq\text{-}DREADD}$ (JAX 026220), *RC::FL*^{hM3Dq} (JAX 026942), *R26*$^{ds\text{-}hM4Di}$ (*52*) and *Ai32*$^{RCL\text{-}ChR2(H134R)/EYFP}$ (JAX 024109) mouse lines were maintained on a mixed genetic background (129/C57Bl6). Both male and female mice were used in this study. Housing, surgery, behavioral experiments, and euthanasia were performed in compliance with Belgian legal guidelines and were approved by the institutional ethical committee of KU Leuven.

Spinal cord transection

Adult mice (P60-90) underwent complete spinal cord transection under isoflurane (1.5%–2%, Iso-Vet) in oxygen-enriched air anesthesia. First, a dorsal midline incision was made, and the musculature covering the dorsal vertebrae was removed to expose the vertebrae. Next, a T7-8 laminectomy was performed to expose the spinal cord, and the spinal cord was transected completely at ~T10 using microscissors. The animals recovered in an incubator maintained at 37°C until fully awake. Analgesia (Metacam, Boehringer Ingelheim, CNK: 2266781, 5 mg/kg) was provided for three days post-surgery for mice that underwent switch trials or training. Animal care, including manual bladder voiding, was performed twice daily. Complete spinal transections were confirmed post-mortem by visual inspection of the spinal cord. Mice were housed on a 12h light/dark cycle with ad libitum access to food and water.

Conditioning paradigm and closed-loop behavioral recordings.

Conditioning trials were performed approximately 24h after the transection surgery. Two randomly assigned mice, a learner, and a control, were tested simultaneously during each trial. The upper bodies of a pair of learner and control mice were restrained separately in custom-designed harnesses with their hindlimbs dangling. We then virtually set the coordinates of their foot marker positions at rest as [x,y,z]=[0,0,0]. Three stainless-steel fine wire electrodes (Crazy Wire Company, SS314-AWG42) were inserted subcutaneously to connect the right tibialis anterior (RTA) of the learner mice to a pulse stimulator (A-M Systems, Model 2100), the right foot of the learner mice with the left foot of the control mice, then the RTA of the control mice to the ground of the stimulator. A criterion to define the stimulation threshold was set at 3mm above the resting position of the hindlimb along the vertical axis (Z), provided that the resting position remained unchanged for about half a minute before each trial. Stimulation intensity was set to 0.177 ± 0.04 mA (10ms pulse duration, 60 Hz constant current

biphasic AC) to induce a standardized limb flexion allowing mice to transiently lift their limb endpoint (the distal end of the fifth metatarsal) above the threshold and to the default resting position below the threshold. The stimulation intensity did not lead to either habituation or sensitization of movements or contribute to the learning rate.

Five IR-reflective markers (3mm hemisphere, B&L Engineering) were placed on the ipsilateral iliac crest, greater trochanter (hip), lateral condyle (knee), malleolus (ankle), and base of the metatarsal phalangeal joint (MTP) of a limb that received electrical stimuli. During each trial, 3D joint positions were recorded with a sampling frequency of 200 Hz using a motion capture system (VICON version 2.12, 5 Vantage cameras), down-sampled to 30 Hz, and analyzed online by custom-written LabVIEW (v19.0 2019 National Instrument) software. A closed-loop system was established by online analysis of kinematic data linked to binary signals (i.e., whether the foot marker is above or below the +3 mm threshold) sent to the microcontroller (Arduino Uno board, ATmega328P). The signals were transformed into transistor-transistor logic (TTL) signals and then to the stimulator. Switch or retrieval experiments were performed approximately 24 hours following the initial acquisition trials. The modified conditioning paradigm was conducted using flexion and extension-based thresholds. In this paradigm, the mouse received conditioning cues whenever its MTP position fell below +2mm or exceeded +4mm from the resting position. Extension and flexion to escape were calculated using the percentage of time spent in the height zone <+2mm and >+4mm ("cue" zone) during the first and last 10% time of the conditioning trial. Mice were excluded when the behavioral training was not reliable.

Kinematic analyses of limb withdrawal and learning phases.

Kinematic data were post-processed offline to reconstruct joint positions and orientation of hindlimb segments. Two sets of parameters were extracted: the limb withdrawal parameters (Table S1, 63 parameters) and the learning parameters (Table S2, 65 parameters). These kinematic parameters were analyzed using principal component analysis (PCA).

The limb withdrawal parameters captured the acute hindlimb movements within 500 ms after each electrical stimulus. The mean position (parameters 1-15), the joint amplitude (16-30), the joint velocity (31-45), the area below the curve (46-60), and the 3D joint angle amplitude (61-63) for each joint along XYZ axes were calculated. The learning parameters captured joint and segment positions over the 600-second trial duration. The mean position (parameters 1-15), the joint amplitude (16-30), the joint velocity (31-45), the area under the curve (46-60), the 3D joint angle amplitude (61-63), the learning outcome (64) and the time spent below the threshold (65) were computed.

Spinal virus injection

Intraspinal injections were performed as previously described (*53*). Briefly, under isoflurane

anesthesia, the dorsal surface of the L3-6 spinal cord segments was exposed. Next, a pulled calibrated borosilicate glass pipette (World precision instruments, TW100-4) was used for the local application of ~100nl AAV9 or DJ8-CAG-FRTed-DTRreverse-WPRE (*54*) (genomic titers >1x10^{13}) virus bilaterally across multiple spinal segments by multiple short pulses (3 ms, 0.4Hz) using an Intracellular microinjection dispense systems (Parker Hannifin, Picospritzer III). Mice were then sutured and underwent post-operative care.

Diphtheria Toxin (DTX) administration for cell type-specific ablation

Diphtheria Toxin (Sigma, D0564, 100mg/kg) was injected intraperitoneally. The toxin was injected two weeks after the injection of AAV-encoding FRT-DTR in the spinal cord. Mice were tested 1-2 weeks after the injection of the Diphtheria toxin. This segmental ablation approach effectively eliminated GeneX-expressing neurons in the lumbar spinal cord (inclusion criteria for behavior > 50% ablation). Our approach to ablate *Ptf1*α^{ON} neurons limited to the lumbar spinal cord did not lead to debilitating scratching behavior known to occur after a systemic ablation of *Ptf1*α-expressing neurons (*55*).

Probe implantation for electrophysiology recording and analyses.

The in vivo awake electrophysiology recording was done one mouse at a time. Learner and control mice were virtually paired by imposing conditioning cue patterns elicited by one learner to another control mouse. Mice were anesthetized with a mixture of Ketamine (Nimatek, Dechra, CNK: 3120-060, 100mg/Kg) and Xylazine (Xyl-M, Livestock Pharma, BE-V170581, 10mg/Kg) or isoflurane (1.5-2%), underwent a complete spinal cord transection (see above), and T12-13 laminectomy was performed to expose L2-6 lumbar segments. A custom-redesigned 3D printed (Objet30 Prime van Stratasys) spinal chamber adapted from (*56*) was used to stabilize the T12-L1 lateral vertebrae and the spinal cord. A duratomy was performed, and an agar pool was placed to keep the spinal cord immersed in ACSF (126µM NaCl, 2.5µM KCl, 2µM $MgSO_4$, 0.07µM NaH_2PO_4, 26µM $NaHCO_3$, 10µM Dextrose, 2µM $CaCl_2$). An Ag/AgCl ground wire (Silver wire 925 coated with AgCl using household bleach, gauge 28) was inserted in the paravertebral muscles adjacent to the laminectomy area. Just before implantation, the recording area of the Neuropixel probe tip (Neuropixel 3A, imec) is immersed in a dye (Disperse Red 1, Sigma, 42364). After the mice were fully awake and using a custom-designed 3D printed probe holder, the Neuropixel probe with 384 channels (dual-band, 0.3-10 kHz and 0.5-500 Hz) was inserted together with an optical fiber (Doric lenses, MFC_060/075-0.37_30mm_ZF1.25_A60) in the spinal cord, approximately 500 µm from the midline and stabilized at ca. 1.5mm deep using a stereotaxic device (Micromanipulator, KOPF, Model 900LS). The hindlimb ipsilateral to the electrode underwent conditioning. Due to noise disturbance with the IR

high-speed cameras and the stimulator (see Conditioning paradigm and closed-loop behavioral recordings above), the closed-loop was established using a two-dimensional digital video image of MTP (30Hz, PlayStation 3 Eye Camera, Sony interactive). Foot position was analyzed online to trigger electrical stimulation (Stimulus Isolator, World precision instruments, A385) using custom software written in Python (v3.8, Continuum Analytics). To synchronize the neuronal recording with the kinematic recording, recording for both systems was triggered simultaneously using an Arduino microcontroller. The conditioning cue frequency was set at 3 Hz during neuronal recording to avoid continuous electrical noise.

The extracellular activity was acquired with a SpikeGLX acquisition board and visualized using SpikeGLX software (v.20190724, Imec phase3A v4.3, https://billkarsh.github.io/SpikeGLX/). Neuronal activity was recorded before (15 mins), during (10 mins), and after (15 mins) of each conditioning trial with minimal neuronal drifting. Opto-tagging was performed for 10 minutes (see Opto-tagging and analysis below). Mice were excluded when no neuronal activity was detected during the baseline recording.

Preprocessing of neural recordings

The recordings were spike-sorted using Kilosort2 (*57*) and manually curated with Phy (*58*) to identify single units. Single units were distinguished from multi-units by imposing a threshold of 10% in the contamination parameter computed by Kilosort2, which is roughly the event rate ratio in the central 2 ms of the clusters' auto-correlogram as pre-set in the clusters' autoclassification function of Kilosort2. The data were then imported in MATLAB (R2020b, 9.9.0 Mathworks) and analyzed using custom-written scripts adapted from the Spikes toolbox (https://github.com/cortex-lab/spikes). To extract the raw spiking activity, spikes were detected using the '*findpeaks'* function of MATLAB using a threshold of 4 standard deviations compared to the signal before the stimulation. Mechanical stability of the recordings, i.e., lack of significant drifting, was verified by visual inspection of drift maps, and dorsal-ventral positions of single units were aligned to the measured insertion depth of the probe. Neurons with an average firing rate of <0.05 spikes/sec across the 40-minute recording were excluded from the analysis. Spikes detected within the ± 1 ms of stimulus cues were indissociable from the stimulation artifact and, therefore, excluded from the study. Dying neurons (neurons with a constant decrease in firing rate from the start of the recording) were manually excluded from the recordings.

Waveform extraction and classification of spinal neurons

Each waveform was extracted using a custom-written MATLAB code. Single units with <0.1 Hz mean firing frequency during the recording (approx. 7 % of isolated units) were not included in the

study. We used previously reported approaches to align, average, and normalize spikes (*59*, *60*). Briefly, we subtracted the mean of the first and last 0.3 ms time window (10 frames) of the spike event, defined as 1.2 ms before and 2.4 ms after the max |peak|, to align waveforms to the baseline. We normalized waveforms by dividing each frame (0.03 ms) by max |peak| of the waveform, such that the maximum deviation is ±1 unit. To temporarily align waveforms, we crop the waveform to -20 to 20 frames from the peak, so each waveform contained 41 time points (i.e., -0.6 ms to 0.6 ms). Waveforms with 1) >2 standard deviations from the first and last baseline means, 2) more than 2 positive peaks or more than 2 negative peaks with predominance of at least 0.1 (*61*), or 3) >0.4 mean difference between the first and last 5 frames (~26% of the isolated units), were excluded. The largest absolute value of a waveform was determined as a depolarization peak. We identified both hypoerpolarizing spikes derived presumably from the cell body (85% of all units) and depolarizing spikes from axons (15% of all units) (*61*). Inclusion or exclusion of depolarizing spikes did not alter the composition of phase tuning units, or differences between learners vs controls. Therefore, all depolarizing spike units are included in Fig 3, 4, S7, S8, and S9.

Single-unit analysis of genetically undefined spinal neurons

Units were identified as modulated during the conditioning when the computed z score was larger than ± two standard deviations (SD) compared to the baseline (10 min pre-conditioning) for at least 20% of the duration of the conditioning. These modulated units were categorized as either "upregulated," "downregulated," or "no change" based on this z-score value. Among the upregulated units, units with an averaged z-score >10 were defined as “highly modulated” units and the Pearson correlation coefficient was computed. Activity variation within the baseline was computed by comparing the z-score of the first and the last 5 minutes of the 15-minute baseline phase. Changes in the z-score transformed firing rates within the conditioning session were quantified by subtracting the averaged z-score of the first 10% of each phase from the last 10% of the same period. Here, we defined 10 mins following the last stimulus cues as the late phase. Units with >1 standard deviation difference from the mean last 10% compared to the first 10% were categorized as increasing or decreasing activity.

Opto-tagging and analysis

Optically tagged single units were identified using 473nm DPSS laser pulses (Laserglow Tech, SN 1610458) by repeated square-pulsed stimulation (100 pulses of 10ms duration, interval 5 ± 1 sec with random jitter, output power 2.5 mW) for 10 min after conditioning trials. Criteria of optically identified single units are the following: a short latency (<7 ms) of first response within a 15 ms window post-stimulation, high consistency of response (>40% of response across trials within the 10

ms window post-stimulation), and increase of averaged Peristimulus Time Histograms (PSTH) within the 15 ms window following stimulation (>2 SD) compared to the averaged PSTH in a 15 ms window before stimulation. Spikes detected ±2 ms for optical stimulation were indissociable from the stimulation artifact and, therefore, excluded from the study. Opto-tagged units (defined as *Ptf1a*-expressing units, as opposed to non-expressing units that were not tagged) were analyzed for direction (up/down) and phase tuning during the trial.

Categorization of input afferent types

We analyzed single-unit responses to stimulus cues within the peristimulus time window (-10 to 60 ms, i.e., a minimum window between two consecutive conditioning cues) during the conditioning trial. To identify a cue-responsive unit, z-scores of the Peristimulus Time Histograms (PSTH) following stimulus cues were computed, and the presence of significant increases in firing rate (>5 SD compared to 10 ms window before stimulation) was identified. We used the following criteria for second-order units: consistency of response to conditioning cues is over 5% of the entire trial, and the jitter of the responses (i.e., the standard deviation of response latency) was shorter than 1 ms (*62*). Non-negative matrix factorization (NNMF) (*63*) were applied to the PSTH of second-order neurons, and units with NNMF peak > 0.5 followed by manual refinement were chosen for further analysis. Second-order unit categorization into Proprioceptive, Aβ, and Aδ/C-fiber afferent input was done using previously described conduction velocity of each afferent type (Proprioception: 20 to 120 m/s Aβ: 12 to 20m/s, Aδ/C: <12m/s); (*64–67*) and estimated distance between stimulation site in the muscles and recording site (5 cm). We combined Aδ and C afferents for most analyses as they both transmit nociceptive afferents and to increase statistical power due to a low number of detected C second-order neurons. A single unit can show multiple responses, in which case, each response is analyzed separately as an individual data point.

Determination of response probability to conditioning cues

For each presumed second-order unit, the response reliability was calculated as % of elicited responses to a given number of conditioning cues. Reliability changes were computed as a difference (Δ) of the probability of the last 10% conditioning cues compared to the first 10%. Outliers (+/- 3 standard deviations) were removed from normally distributed datasets. We classified units with a |delta| greater than 0.05 as changing their response probability, and the rest were defined as "no change". A non-parametric bootstrapping method (*68*, *69*) was used to validate the results *in silico*. We resampled the original data ten times for each population and randomly selected n points with replacement, extracted the mean for each iteration, and stored it in an array by repeating the process multiple times. To determine the change in response probability across cues with respect to learning

criterion, response probabilities were averaged across 10 bins of 10% of the total amount of cues/mouse. The effect size was calculated using a non-parametric Cliff's delta to quantify the difference between the two groups (*70*), and the statistical power was then computed on the raw and the bootstrapped data.

Pharmacogenetic manipulations

For pharmacogenetic silencing ($R26^{ds\text{-}hM4di}$) and activation ($R26^{LSL\text{-}hM3Dq}$ or $RC::FL^{hM3Dq}$) experiments, all mice received i.p. injections of C21 (1 mg/kg; Tocris Bioscience, dissolved in 5% DMSO) 30 mins before behavioral testing.

Immunohistochemistry

After the behavioral and electrophysiological tests, all mice were anesthetized with a mix of Ketamine (100 mg/kg, intraperitoneally) and Xylazine (5mg/kg, intraperitoneally) and perfused with 4% paraformaldehyde. The tissue was post-fixed either 4 hours or overnight, cryoprotected in 30% sucrose/PBS, and cryosectioned (40-60 µm transverse sections). Free-floating sections were blocked in a solution containing 1% BSA and 0.1-0.4% Triton X-100 diluted in PBS 0.01M, followed by incubation with primary antibodies overnight (or 3 nights for ChAT) at 4°C. The following primary antibodies were used: Chicken anti-*ß*-galactosidase (1:5000, Abcam, AB9361, RRID: AB_307210), Chicken anti-GFP (1:1000, Thermo Fisher Scientific, A10262, RRID: AB_2534023), Goat anti-ChAT (1:1000, Sigma-Aldrich, AB144P, RRID: AB_2079751), Mouse anti-RFP (1:2000, MBL, M155-3). The following secondary antibodies were used: Alexa Fluor donkey anti-chicken 488 (Jackson ImmunoResearch, 703-545-155), Alexa Fluor donkey anti-goat Cy3 (Jackson ImmunoResearch, 705-165-147), Alexa Fluor donkey anti-goat Cy5 (Jackson ImmunoResearch, 705-605-147), DyL405 Donkey anti-guinea pig (Jackson ImmunoResearch , 706-475-148), Donkey anti-guinea pig Cy3 (Jackson ImmunoResearch, 706-475-148), Alexa Fluor donkey anti-guinea pig Cy5 (Jackson ImmunoResearch, 706-605-148), Donkey anti-mouse Cy3 (Jackson ImmunoResearch, 715-165-150), Alexa Fluor donkey anti-mouse Cy5 (Jackson ImmunoResearch, 715-605-150), Alexa Fluor donkey anti-rabbit 488 (Molecular Probe, A11055), Donkey anti-rabbit Cy3 (Jackson ImmunoResearch, 711-165-152), Alexa Fluor donkey anti-rabbit Cy5 (Jackson ImmunoResearch, 711-605-152), DAPI (Sigma, D9542) was used to stain cell bodies.

Spinal cord reconstructions and quantifications

Spinal cord images were acquired using a confocal (Zeiss, 10x objective). Positions of LacZ-expressing neurons were reconstructed and quantified using ImageJ (Fiji, https://fiji.sc/) or Imaris (BitPlane, Inc). Custom-written R scripts (The R project, https://www.r-project.org/) were used to

visualize data. DTX ablation efficiency was calculated by comparing the total LacZ-expressing neural density between intact and ablated mice from the same genotype. We set the inclusion criteria to be > 50% ablation of *PD*-expressing neurons over spinal segments that span 200 μm by the center of ablation (L4-6).

Statistical analysis

Mice with appropriate genotypes were randomly allocated to different groups for the electrophysiological and behavioral experiments. Group sizes were not pre-determined, but sample sizes were comparable to those commonly used for similar experiments and were selected such that appropriate statistical tests could be used. Data analysis for extracellular recording was blinded as much as possible. For behavioral kinematics, data collection and analysis were automated, minimizing any potential influence by the experimenter. For *in-vivo* electrophysiology, the data were included in the analyses in all cases where good recordings were obtained. Animals were only excluded from behavioral experiments if data collection could not be performed, i.e., mice did not reliably perform the conditioning. Normality was assessed using the Shapiro-Wilk test, and non-parametric tests were used for non-normally distributed data. All parametric and non-parametric tests used, as well as any multiple comparisons tests and corrections, are indicated below, and n values for each experiment in the figure legends. Values are reported as mean ± standard error of the mean (S.E.M) for Figures 1E, 2E, 3G, S2B, S2D, S2F, S3D-F, S4B, S4D-E, S5A, S6F, and S9E, except for Figures 1D, 1G, 2D, S2A, S3C, S3G and S4C, where values are reported as mean ± standard deviation (SD), for Figure 4E, where values are reported as median ± quartiles, and for Figure 4D, 4G, and S11B-C where values are reported as median± range. Statistical analyses were performed using Prism 8 (v8.2.1 GraphPad) or MATLAB (version 2017b or 2020). The normality of the distributions was systematically verified, and the statistical tests were chosen accordingly. Statistical tests used in this study include Student's paired *t*-test (Fig. 1E, 1H, S2B, S2F, S2G, S3D, S3H, S9E, S10B), Student's unpaired two-sample *t*-test (Fig. 2E, 4G, S3D, S4E, S5A, S11B-C), Wilcoxson matched-paired signed rank test (Fig. 5D, 5G, 5I, S2F, S2G, S3E, S3F, S3H), Mann-Whitney test (Fig. 3G, 4D, 5D, S3E, S3F, S4D, S6F), Pearson's chi-squared test (Fig. 4D, 4G, 4I, S7A, S8C, S9C), ANOVA or Kruskal Walis test for repeated measurement and Dunn-Sidak posthoc test for non-parametric multiple comparisons (Fig. 4E), Chi-squared distribution test (Fig. S8D). The significance level is defined as follows for all analyses performed: *$p< 0.05$; **$p< 0.01$; ***$p< 0.001$, and all significant P values are indicated in figure legends.

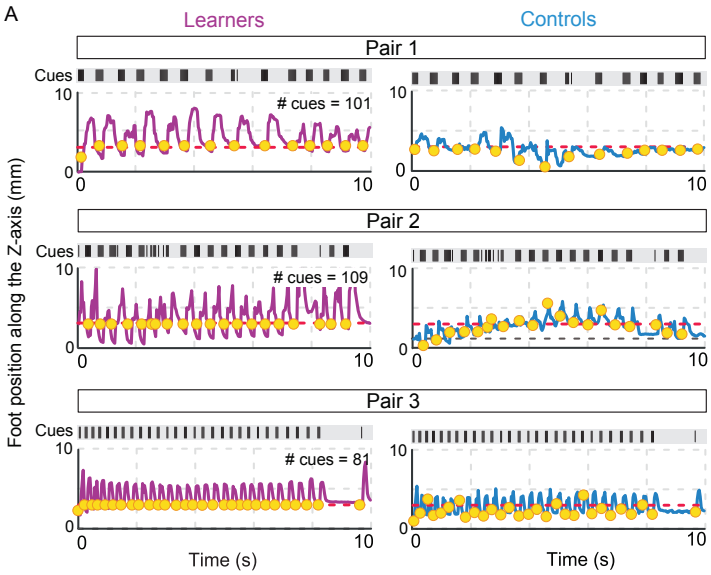

Fig. S1. Example of learner-control pairs.

(A) Example foot traces of the first 10 seconds of 3 pairs of learners (magenta) and controls (cyan). Solid black lines indicate the moment in which conditioning cues are elicited. Yellow dots show foot positions when conditioning cues are elicited.

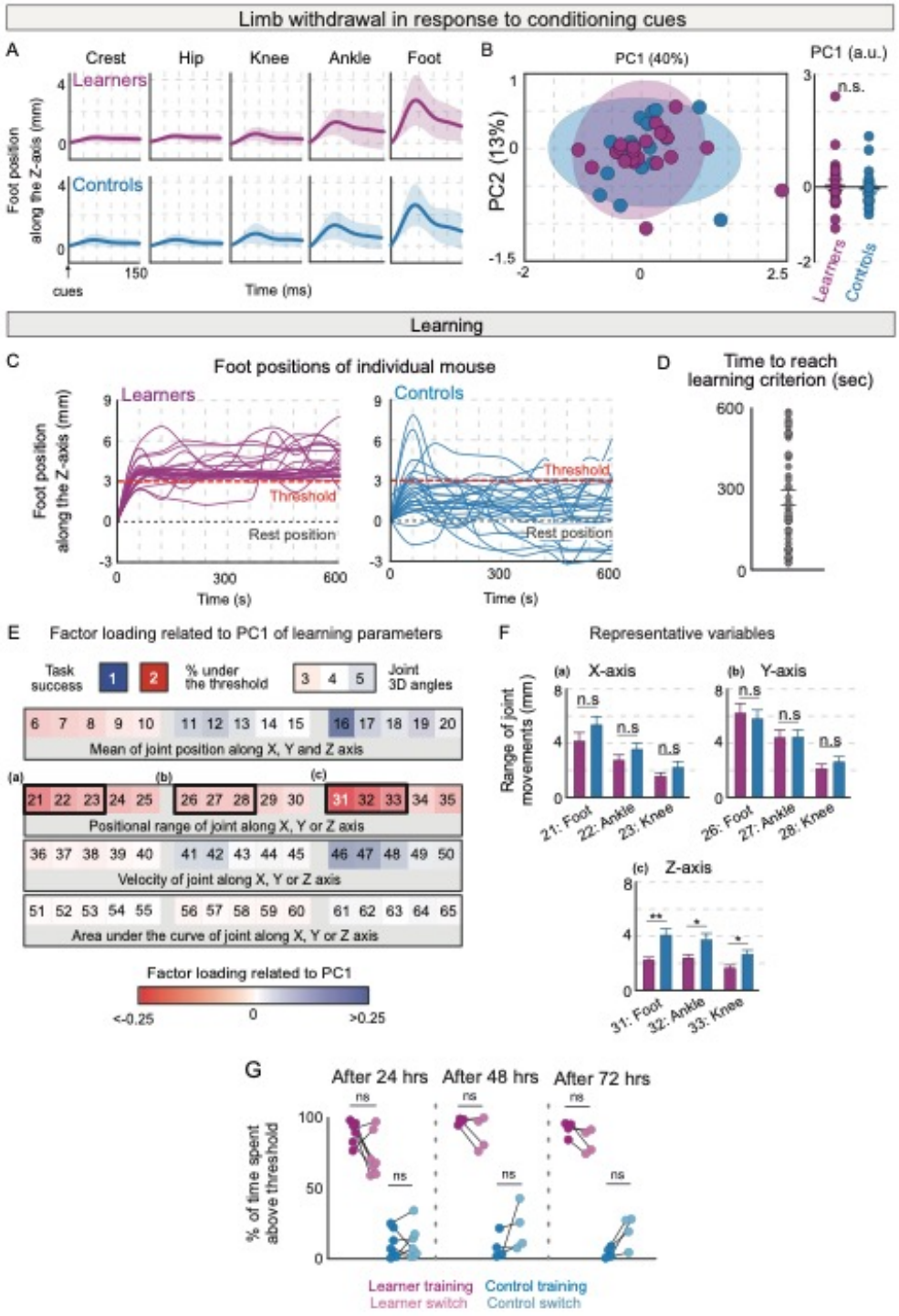

Fig. S2. Kinematic analyses of spinal instrumental learning.

(A) Mean joint kinematics of learner (magenta) and control (cyan) mice (n=25 in each group) in response to conditioning cues. 0 indicates the normalized position of each joint at the time of stimulation. The data is up-sampled to 300 Hz and smoothed. The shaded area represents 1 SD.

(B) PC analysis describing hindlimb movements in response to conditioning cues (each dot represents one mouse, n=25 each) in the new PC1-2 space. Least-square elliptical fitting (95% confidence)

shows the lack of differences between the two experimental groups. Histogram plot reports mean values of measured PC1 scores (Student's paired *t*-test, $p>0.05$).
(C) Individual traces of learner (magenta) and control (cyan) foot positions along the Z-axis during 10-minute conditioning trials (n=25 each). Sampling rate: 1 Hz and smoothed using a Gaussian filter for visualization.
(D) Histogram of the time required to reach the learning criterion. The time (seconds) in which 90% of conditioning cues were delivered is shown.
(E) Learning kinematic parameters correlated with PC1 (factor loading >|0.25|) are shown in darker shades of blue or red. The numbers correspond to Table S2.
(F) Histogram plots reporting mean values for representative variables of functional clusters that differentiate learner to control mice (n=25 each). Error bars represent SEM (Wilcoxson matched-paired signed rank test or Student's paired t-test, $*p<0.05$, $**p<0.01$).
(G) Training imposed 48 or 72 hours after spinal transection followed by reversal learning leads to proactive interference, irrespective of possible injury-induced acute network level adaptation (n=7 for 24h, n=4 for 48h and n=4 for 72h, Wilcoxson matched-paired signed rank test or Student's paired t-test, $p>0.05$).

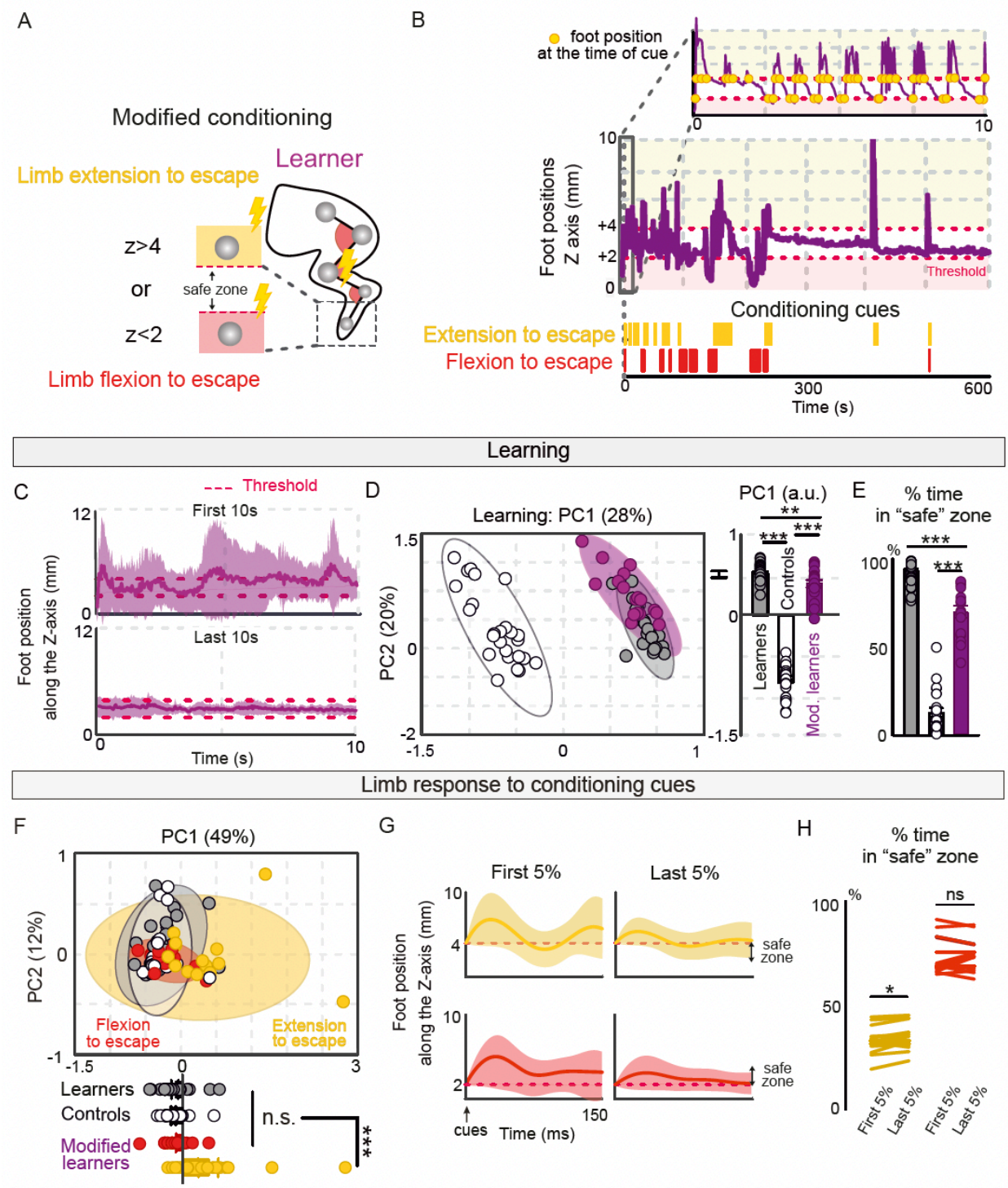

Fig. S3. Cues that impose limb extension, in addition to flexion, can elicit spinal conditioning.

(A) Scheme of contingency between limb position and conditioning cues.
(B) Representative reconstructions of foot positions for a learner during a modified conditioning session. Red dotted lines indicate the +2 or 4 mm conditioning cue threshold. The insets show the first 10 sec of the session. The data is down-sampled to 1Hz for visualization. Yellow dots show foot positions when conditioning cues are elicited.
(C) Mean foot position during the first and last 10 seconds of the modified conditioning trial along the Z-axis (n=18 each). A red dotted line indicates the conditioning cue threshold; 0 shows the resting

position at the beginning of a trial. The data is down-sampled to 1Hz. The shaded area represents 1 SD.
(D) PC analysis describes features of the limb kinematics in the new PC1-2 space for learning (each dot represents one mouse, gray: learners white: controls n=25 each, magenta: learners in modified conditioning, n=18). Least-square elliptical fitting (95% confidence) is shown. Histogram plot reporting mean values of measured PC1 scores (Student's paired and unpaired t-test, $**p<0.01$, $***p<0.001$).
(E) Percentage of time spent in the safe zone: foot position >3 mm for the conventional conditioning, and 2< foot position < 4 mm for the modified conditioning during the conditioning sessions. Modified conditioning is more challenging than conventional conditioning, yet learners from modified conditioning exhibit clear learning behavior (Wilcoxson matched-paired signed rank test or Mann-Whitney test, $***p<0.001$).
(F) PC analysis describing hindlimb movements in response to conditioning cues (each dot represents one mouse, gray: learners white: controls n=25 each, red: learners in modified conditioning for the lower threshold, yellow: the same set of learners in modified conditioning for the upper threshold, n=18) in the new PC1-2 space with least-square elliptical fitting (95% confidence). Histogram plot reports mean values of measured PC1 scores (Wilcoxson matched-paired signed rank test or Mann-Whitney test, $***p<0.001$).
(G) Foot traces in response to conditioning cues to +2 and +4 mm thresholds from the first and last 5% of individual mice (n=18). The data is up-sampled to 300 Hz and smoothed. The shaded area represents 1 SD. The thick lines indicate the mean.
(H) An increase in time spent in the safe zone (2< foot position < 4 mm) of the first and last 5% of the trial (1 min each) for extension-based escape (left) but not flexion-based escape (right) demonstrates mice position foot into the safe zone as the learning progresses (Student's paired *t*-test or Wilcoxson matched-paired signed rank test, $*p<0.05$).
Error bars represent SEM.

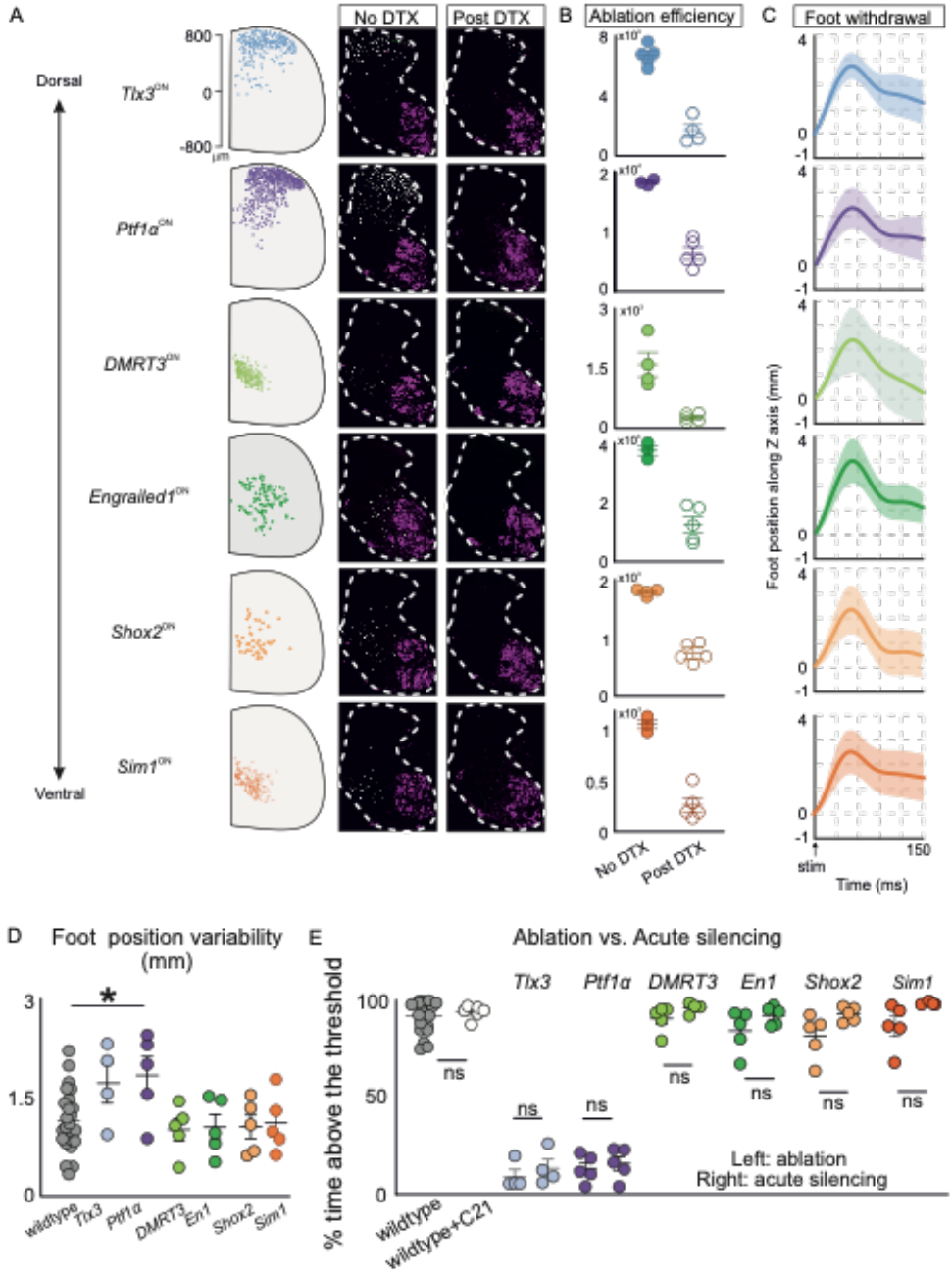

Fig. S4. Efficient cell type-selective ablation and the foot withdrawal kinematics.

(A) Left: Reconstruction of *β*-galactosidase-expressing cells in a 60 μm coronal spinal section. Half of the spinal cord is shown. Right: Representative confocal images of genetically marked cell types of interest (*β*-galactosidase-expressing cells; white dots, ChAT-positive motor neurons; magenta) in intact and PD^{DTX} lumbar spinal cords (~L5).

(B) Quantification of ablation efficiency between intact and PD^{DTX} learner mice. We set the inclusion criteria to be > 50% ablation of PD^{ON} neurons. Mean ablation efficiencies: $Tlx3^{DTX}$ 76%, $Ptf1\alpha^{DTX}$ 65%: $DMRT3^{DTX}$ 83%, $En1^{DTX}$ 63%, $Shox2^{DTX}$ 52%, and $Sim1^{DTX}$ 74%). Each dot indicates one mouse.

(C) Mean foot joint movements along the Z-axis during the limb withdrawal in response to conditioning cues after ablation (n=5 for each group except n=4 for the $Tlx3^{DTX}$ group). 0 indicates a

normalized resting foot position at the beginning of the trial. The shaded area represents 1 SD. Kinematic data were up-sampled to 300 Hz.

(D) Foot flexion variability is not different between wild-type and PD^{DTX} learners (Mann-Whitney test, $^{**}p<0.01$).

(E) Ablation and acute silencing of PD neurons leads to the same conclusion, i.e., *Tlx3*- and *Ptf1α*-expressing neurons are the populations critical for the conditioning behavior (Student's unpaired two-sample t-test, $p>0.05$).

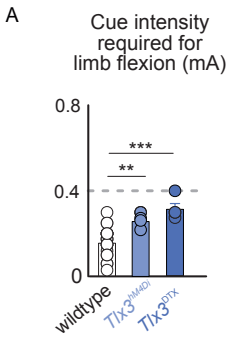

Fig. S5. Silencing of *Tlx3*-expressing neurons leads to hyposensitivity to conditioning cues.

(A) *Tlx3*^{hM4Di} *and Tlx3*^{DTX} mice require a higher intensity of conditioning cues to elicit limb flexion compared to wild-type learners (Student unpaired two-sample t-test or Mann-Whitney test, $^{**}p<0.01$, $^{***}p<0.001$).

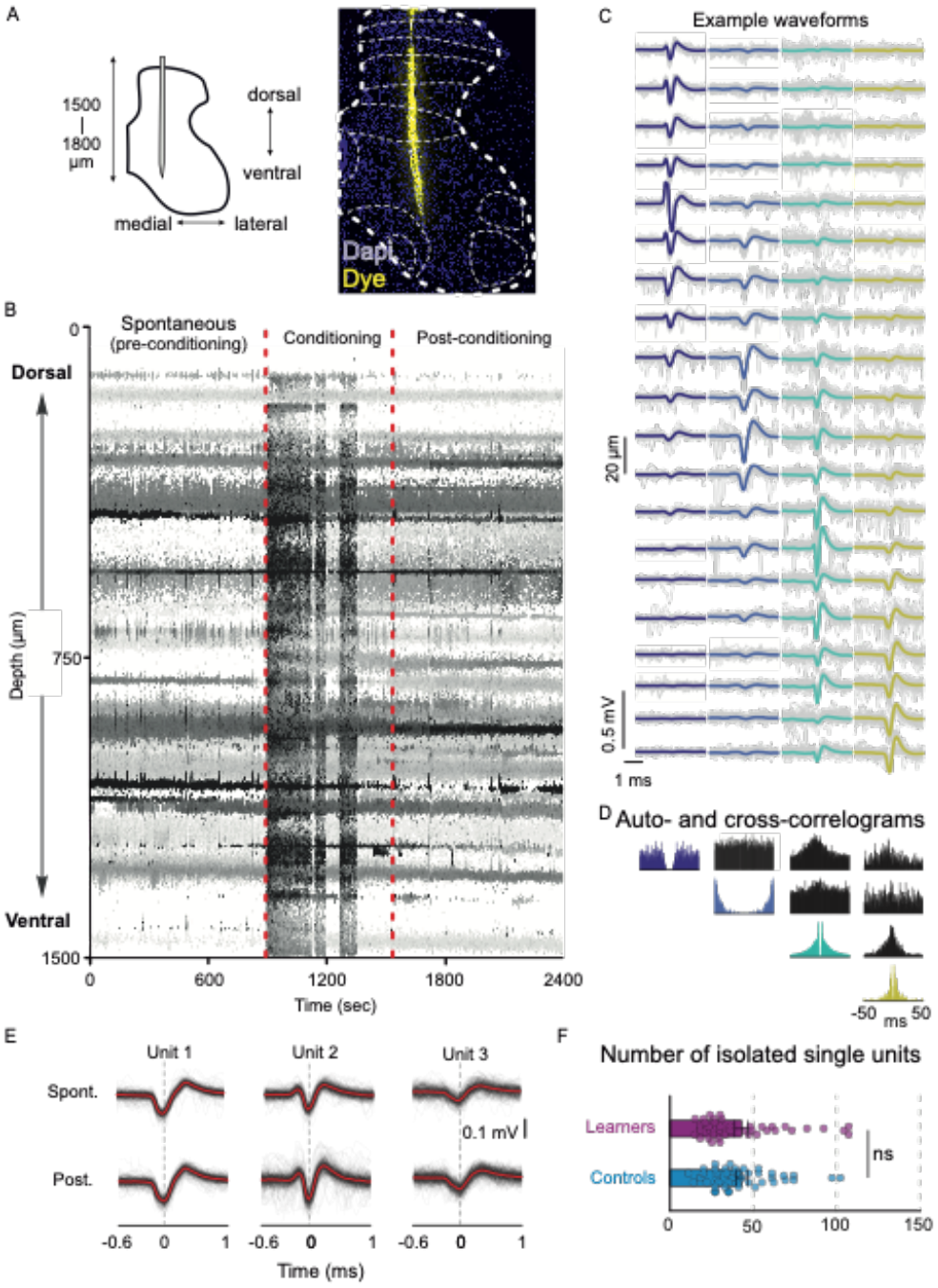

Fig. S6. *In vivo* spinal electrophysiological approach in awake behaving mice.

(A) Representative histological image of the electrode placement in the spinal cord. Half of the spinal cord is shown.

(B) Example of the absence of neuronal drifting, before (15 min), during (10 min), and after (15 min) a single conditioning trial. A darker color indicates more considerable changes in firing rate. Red dotted lines indicate the beginning and the end of the conditioning trial.

(C) Example spike waveforms from four selected neurons recorded on overlapping channels. The mean waveform (color) is overlaid on 50 randomly selected individual waveforms (gray). The scale bar indicates the distance between recording sites.

(D) Auto- and cross-correlograms (colored and black plots, respectively) of the example neurons, shown over a −50 to +50 ms window.
(E) Example units with the first and last 300 spike waveforms indicate the stability of recordings.
(F) The mean number of isolated units per recording does not differ between learners and controls. Each dot represents one mouse (n=40 for both groups; Mann-Whitney test, $p>0.05$).

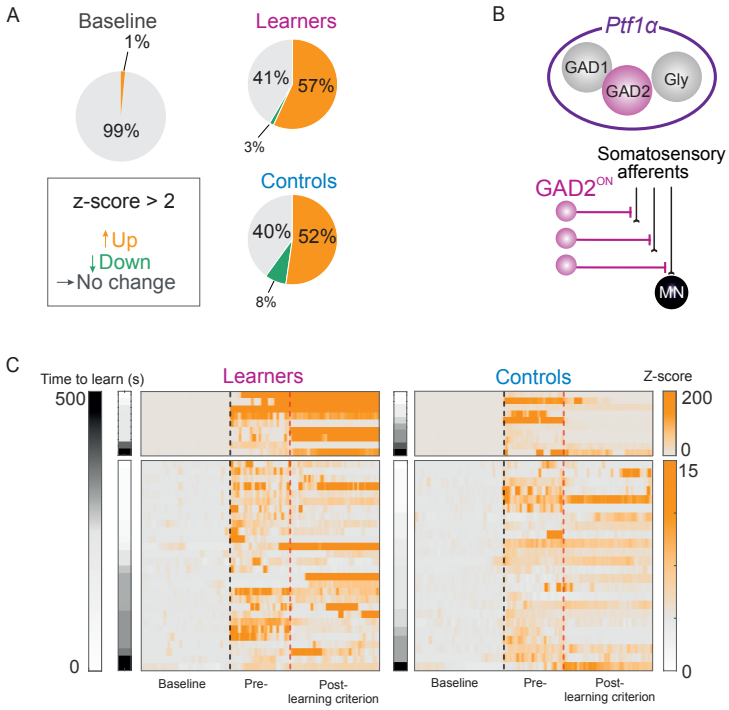

Fig. S7. The proportion of activity-modulated *Ptf1a*-expressing neurons is similar between learner and control groups.

(A) The proportion of units with upregulated, downregulated, or no change in activity compared to the baseline (up or down-regulated: z-score > |2| compared to the baseline, n= 65 units for both learners and controls). A similar proportion, approximately 60% of *Ptf1α*-expressing units, show activity modulation during the conditioning in learners and controls (Pearson's chi-squared test, p>0.05).

(B) Summary scheme of heterogeneous *Ptf1α*-expressing population.

(C) Heatmap of the *Z*-score transformed firing rate of every optotagged *Ptf1α*-expressing unit before and during conditioning. To visualize activity changes, the z-axis has been time-warped to align the learning criterion (red vertical line). Units are presented from top to bottom in the order of shortest to longest time in which the learning criterion was met. The top panels represent the units with the highest z-score (Average Z-score>10) during the pre-learning criterion.

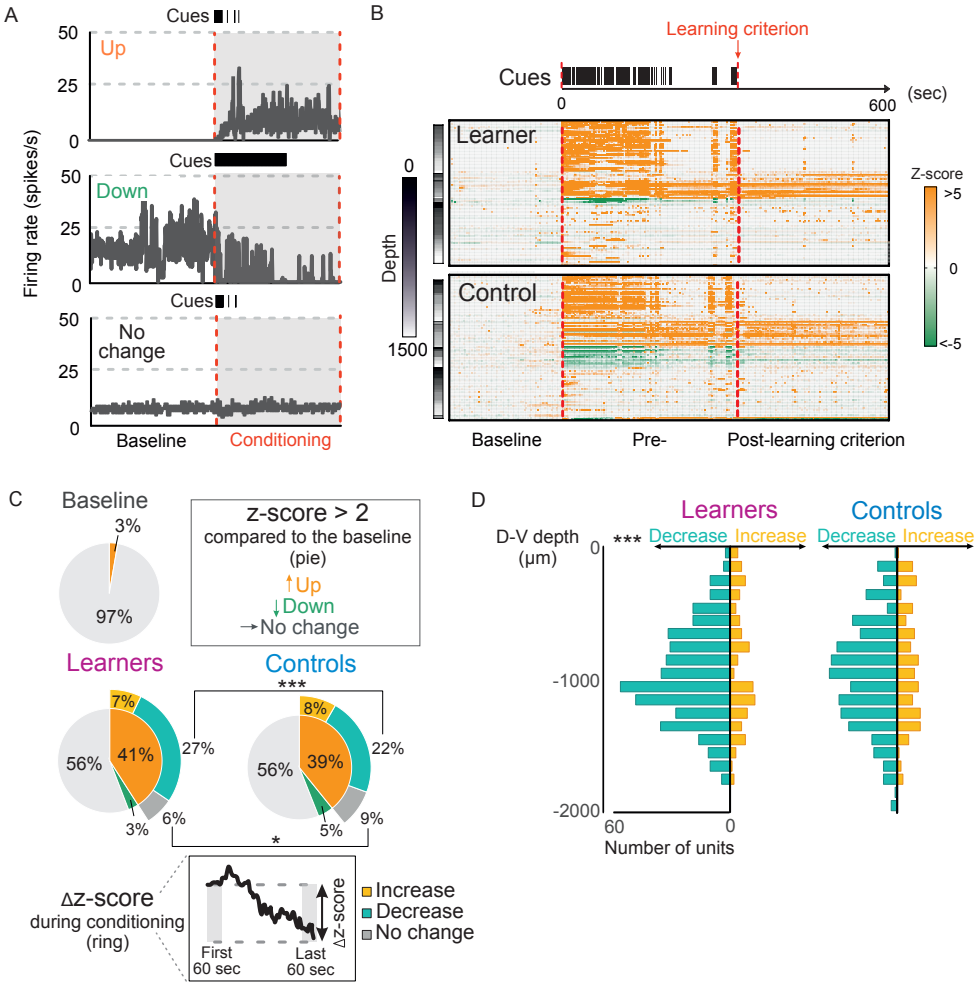

Fig. S8. Activity dynamics of *Ptf1a*-negative units differ between learner and control groups.

(A) Example units exhibiting up (top), downregulation (middle), and no change (bottom) of activity aligned to conditioning cues (black vertical line) during the conditioning trial. Shaded windows indicate the conditioning period.

(B) Top: Definition of pre (the period with conditioning cues) and post (no cues) learning criterion. Bottom: Activity heatmap of a representative pair of a learner and a control (n= 59, 55 units, respectively) with rows displaying the *Z*-score-transformed firing rate of individual neurons and columns representing time before (200 sec) and during the session (600 sec, 3-sec bin). Approximately 50% of units show activity modulation during the conditioning.

(C) The proportion of upregulated or downregulated activity compared to the baseline in learner (1509 units) and control (1526 units) mice (pie; n=40 for each group). No difference is found between learners and controls. Of the upregulated units, there are more units exhibiting decreasing activity over the course of the session (ring; Pearson's chi-squared test, *p<0.05, ***p<0.001, the bottom inset with schematized data).

(D) Spatial locations of upregulated units compared to the baseline showing significant activity modulation within the session (Chi-squared distribution test, ***p<0.001).

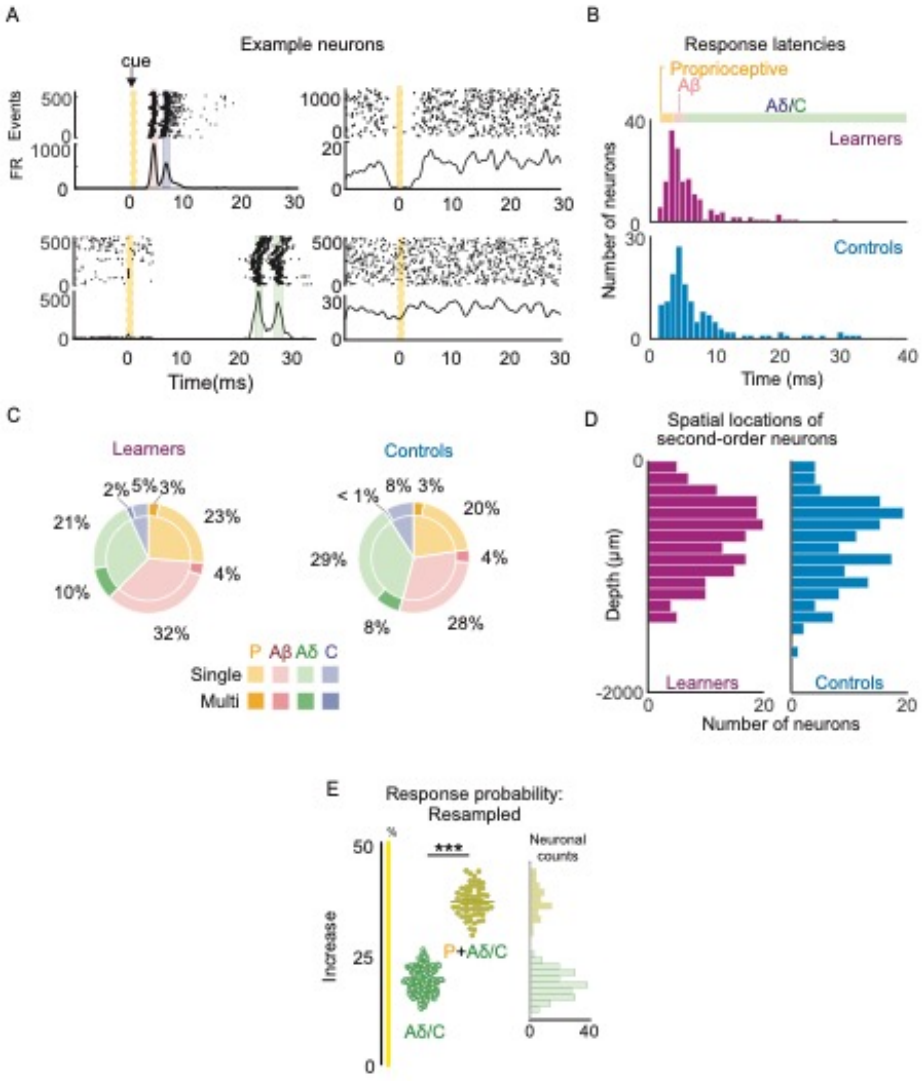

Fig. S9. The composition of second-order neurons is similar between learners and controls.

(A) Example second-order neurons and their response patterns to conditioning cues. Two units (left) show two distinct monosynaptic responses to conditioning cues (Approximately 20% of total second-order neurons). Some units are inhibited in response to cues (top right) or non-responsive (bottom right).

(B, C) The distribution of response latency (B) and the proportion of second-order units (C) is categorized by their input from presumed proprioception, Aβ, Aδ/C afferents in learners and controls (learners n= 152 units, n=173 responses, controls n=130 units, n=142 responses). A large proportion of neurons (~80%) displayed responses at one latency, but some (~20%) exhibited multiple responses to condition cues, including different types of afferent input from distinct somatosensory modalities. No difference is found between learners and controls (Pearson's chi-squared test, p>0.05).

(F) Spatial distribution of second-order neurons in learners and controls.

(G) Resampled (10 times) data showing the statistical difference between Aδ/C and P+Aδ/C second-order neurons exhibiting increased response probability, with effect size (Cliff's delta) of 0.992, with a statistical power of 0.99.

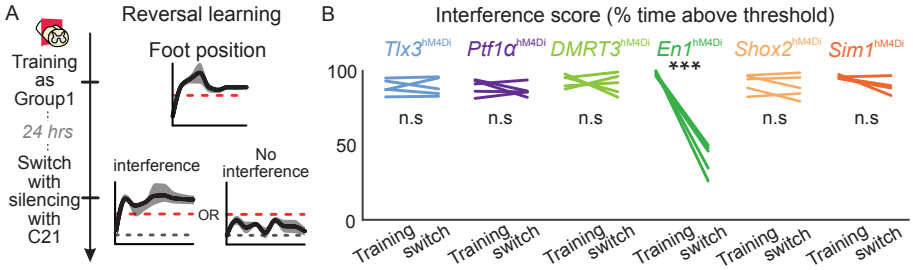

Fig. S10. *En1* ablation disrupts learning interference of previously conditioned behavior.

(A) Experimental timeline of mice with *PD*-expressing neurons expressing hM4Di-DREADD inhibitor undergoing reversal learning as the Group 1 and possible outcomes. Red dotted lines indicate the conditioning cue threshold.

(B) Interference score (% time spent above the threshold during switch trials) of *PD*-expressing neurons expressing hM4Di-DREADD inhibitor (*Tlx3*^{hM4Di} n=5, *Ptf1α*^{hM4Di} n=8, *DMRT3*^{hM4Di}, n=5, *En1*^{hM4Di} n=5, *Shox2*^{hM4Di} n=5, *Sim1*^{hM4Di} n=4, Student's paired *t*-test, ***$p<0.001$, $p>0.05$).

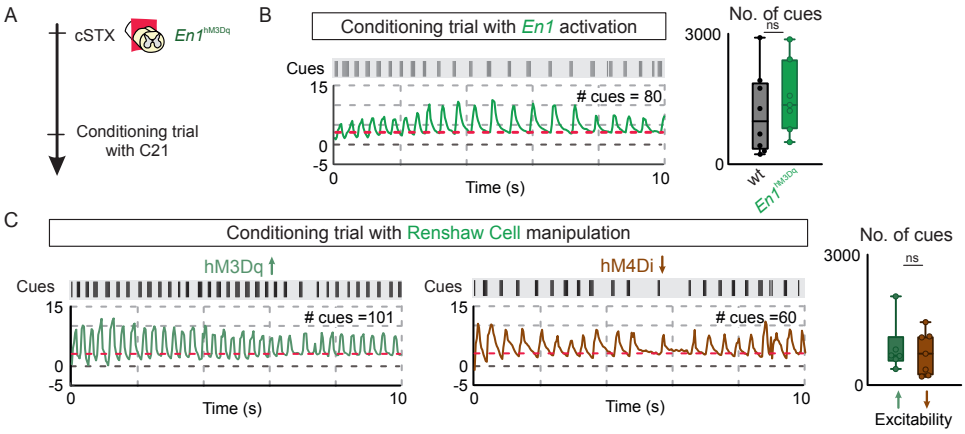

Fig. S11. Manipulating the excitability of *En1*-expressing neurons and their subpopulation during the conditioning trial does not influence the learning process.

(A-C) Experimental design and an example foot traces of the first 10 seconds during the conditioning trial while manipulating excitability of *En1*-expressing (A, B; wildtype n=8 *En1*^{hM3Dq} +C21 n=7; two-sided t-test) or Renshaw cells (C; *En1*^{hM3Dq} +C21 n=6, CB::*En1*^{hM4Di} +C21 n=7; Student's unpaired two-sample t-test) and the number of conditioning cues required to reach the learning criterion. Median± range is shown.

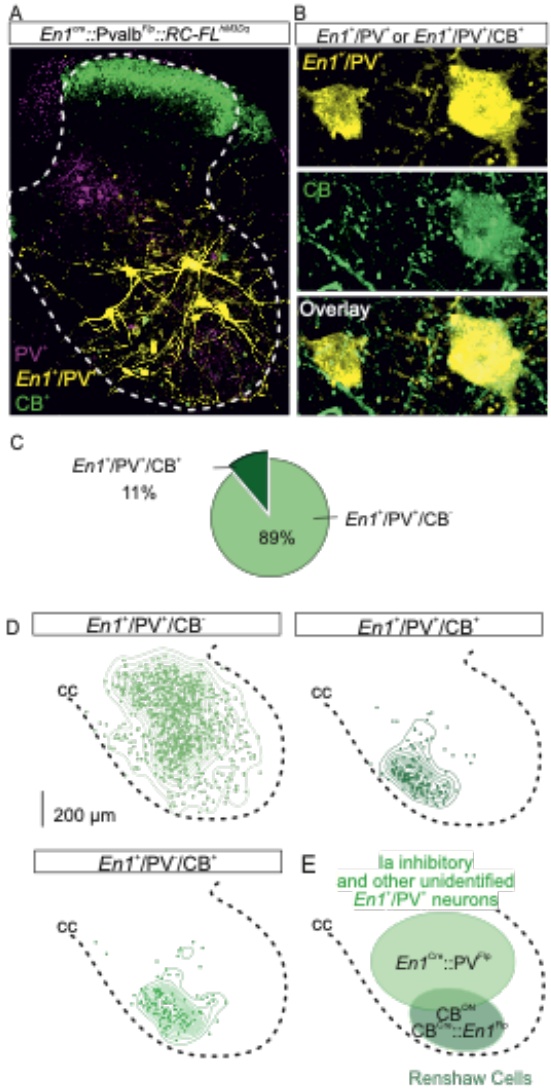

Fig. S12. The proportion of PV/CB-expressing population among PV-expressing neurons.

(A) Representative image of *En1*/Parvalbumin (PV)-expressing neurons (yellow) expressing hM3Dq-DREADD activator in the lumbar spinal cord. Magenta: PV-expressing only, Green: Calbindin (CB)-expressing neurons

(B) Immunohistochemical image of *En1/PV*-expressing neurons, some of which express Calbindin.

(C) The proportion of PV-only and PV/CB-expressing neurons, both of which are subpopulations of *En1*-expressing neurons.

(D-E) Spatial positioning of PV-, CB-, or PV/CB-expressing neurons, and presumed Ia inhibitory neurons (Ia; light green) plus other unidentified *En1*/PV-expressing neurons and Renshaw Cells (dark green).

Table S1.

Limb withdrawal parameters used for kinematic analysis.

MEAN JOINT POSITION (mm)	
1	Foot position along X-axis
2	Ankle position along X-axis
3	Knee position along X-axis
4	Hip position along X-axis
5	Iliac crest position along X-axis
6	Foot position along Y-axis
7	Ankle position along Y-axis
8	Knee position along Y-axis
9	Hip position along Y-axis
10	Iliac crest position along Y-axis
11	Foot position along Z-axis
12	Ankle position along Z-axis
13	Knee position along Z-axis
14	Hip position along Z-axis
15	Iliac crest position along Z-axis

MEAN JOINT VELOCITY (mm/s)	
31	Foot speed along X-axis
32	Ankle speed along X-axis
33	Knee speed along X-axis
34	Hip speed along X-axis
35	Iliac crest speed along X-axis
36	Foot speed along Y-axis
37	Ankle speed along Y-axis
38	Knee speed along Y-axis
39	Hip valong Y-axis
40	Iliac crest speed along Y-axis
41	Foot speed along Z-axis
42	Ankle speed along Z-axis
43	Knee speed along Z-axis
44	Hip speed along Z-axis
45	Iliac crest speed along Z-axis

POSITIONAL RANGE OF JOINT (mm)	
16	Max - Min of foot along X-axis
17	Max - Min ankle along X-axis
18	Max - Min knee along X-axis
19	Max - Min hip along X-axis
20	Max - Min iliac crest along X-axis
21	Max - Min foot along Y-axis
22	Max - Min ankle along Y-axis
23	Max - Min knee along Y-axis
24	Max - Min hip along Y-axis
25	Max - Min iliac crest along Y-axis
26	Max - Min foot along Z-axis
27	Max - Min ankle along Z-axis
28	Max - Min knee along Z-axis
29	Max - Min hip along Z-axis
30	Max - Min iliac crest along Z-axis

ABSEMENT OF JOINT DISPLACEMENT (mm.s)	
46	Area under the response movement of the foot along X-axis
47	Area under the response movement of the ankle along X-axis
48	Area under the response movement of the knee along X-axis
49	Area under the response movement of the hip along X-axis
50	Area under the response movement of the iliac crest along X-axis
51	Area under the response movement of the foot along Y-axis
52	Area under the response movement of the ankle along Y-axis
53	Area under the response movement of the knee along Y-axis
54	Area under the response movement of the hip along Y-axis
55	Area under the response movement of the iliac crest along Y-axis
56	Area under the response movement of the foot along Z-axis
57	Area under the response movement of the ankle along Z-axis
58	Area under the response movement of the knee along Z-axis
59	Area under the response movement of the hip along Z-axis
60	Area under the response movement of the iliac crest along Z-axis

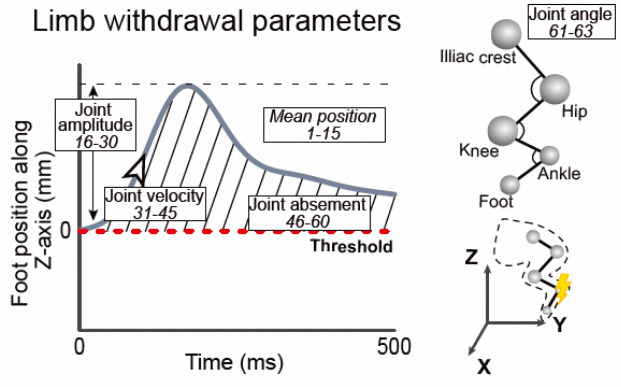

JOINT ANGLE (°)	
61	Max - Min of the 3D foot angle
62	Max - Min of the 3D ankle angle
63	Max - Min of the 3D knee angle

Table S2.

Learning parameters used for kinematic analysis.

PERFORMANCE SCORE	
1	Last 60 seconds of each trial (binary: 0.1: above/below threshold)
2	Time spent below the 3mm threshold (%)

JOINT ANGLE (°)	
3	Max - Min of the 3D foot angle
4	Max - Min of the 3D ankle angle
5	Max - Min of the 3D knee angle

MEAN JOINT POSITION (mm)	
6	Foot position along X-axis
7	Ankle position along X-axis
8	Knee position along X-axis
9	Hip position along X-axis
10	Iliac crest position along X-axis
11	Foot position along Y-axis
12	Ankle position along Y-axis
13	Knee position along Y-axis
14	Hip position along Y-axis
15	Iliac crest position along Y-axis
16	Foot position along Z-axis
17	Ankle position along Z-axis
18	Knee position along Z-axis
19	Hip position along Z-axis
20	Iliac crest position along Z-axis

POSITIONAL RANGE OF JOINT (mm)	
21	Max - Min of foot along X-axis
22	Max - Min ankle along X-axis
23	Max - Min knee along X-axis
24	Max - Min hip along X-axis
25	Max - Min iliac crest along X-axis
26	Max - Min foot along Y-axis
27	Max - Min ankle along Y-axis
28	Max - Min knee along Y-axis
29	Max - Min hip along Y-axis
30	Max - Min iliac crest along Y-axis
31	Max - Min foot along Z-axis
32	Max - Min ankle along Z-axis
33	Max - Min knee along Z-axis
34	Max - Min hip along Z-axis
35	Max - Min iliac crest along Z-axis

MEAN JOINT VELOCITY (mm/s)	
36	Foot speed along X-axis
37	Ankle speed along X-axis
38	Knee speed along X-axis
39	Hip speed along X-axis
40	Iliac crest speed along X-axis
41	Foot speed along Y-axis
42	Ankle speed along Y-axis
43	Knee speed along Y-axis
44	Hip valong Y-axis
45	Iliac crest speed along Y-axis
46	Foot speed along Z-axis
47	Ankle speed along Z-axis
48	Knee speed along Z-axis
49	Hip speed along Z-axis
50	Iliac crest speed along Z-axis

ABSEMENT OF JOINT DISPLACEMENT (mm.s)	
51	Area under the response movement of the foot along X-axis
52	Area under the response movement of the ankle along X-axis
53	Area under the response movement of the knee along X-axis
54	Area under the response movement of the hip along X-axis
55	Area under the response movement of the iliac crest along X-axis
56	Area under the response movement of the foot along Y-axis
57	Area under the response movement of the ankle along Y-axis
58	Area under the response movement of the knee along Y-axis
59	Area under the response movement of the hip along Y-axis
60	Area under the response movement of the iliac crest along Y-axis
61	Area under the response movement of the foot along Z-axis
62	Area under the response movement of the ankle along Z-axis
63	Area under the response movement of the knee along Z-axis
64	Area under the response movement of the hip along Z-axis
65	Area under the response movement of the iliac crest along Z-axis

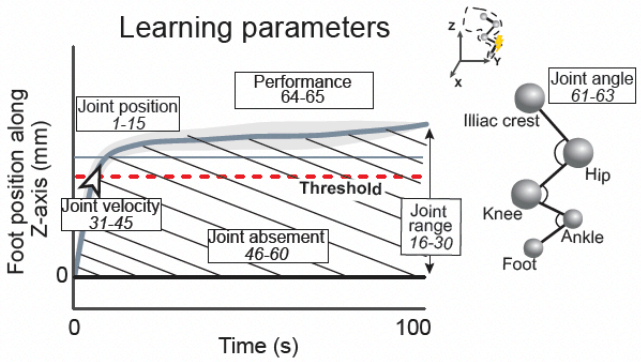

Movie S1.

A representative learner and control pair and their foot position during the first 10 seconds of the conditioning session. Speed is slowed down by a factor of three.